FINAL TECHNICAL REPORT

Project Title: Spray Rolling Aluminum Strip

Covering Period: February 04, 2000 through September 30, 2005

Recipient: University of California, Irvine (UCI)
160 Administration Building
Irvine, CA 92697

Award Number: DE-FC36-00ID13816

Principal Investigator: Enrique J. Lavernia
University of California, Davis (UCD)
College of Engineering
Davis, CA 95616-5294
Tel: (530) 752-0554; Email: lavernia@ucdavis.edu

Co-PIs: Jean-Pierre Delplanque
(Formerly with the Colorado School of Mines)
University of California, Davis (UCD)
College of Engineering
Davis, CA 95616-5294

Kevin M. McHugh
Idaho National Laboratory (INL)
Idaho Falls, ID 83415

Other Partners: Alcoa Technical Center

Pechiney Rolled Products

Inductotherm Corp.

Metal Technology, Inc.

Acknowledgement: This material is based upon work supported by the U S. Department of Energy under Award No. DE-FC36-00ID13816.

Table of Contents

List of Figures

List of Tables

I. Executive Summary

Spray forming is a competitive low-cost alternative to ingot metallurgy for manufacturing ferrous and non-ferrous alloy shapes. It produces materials with a reduced number of processing steps, while maintaining materials properties, with the possibility of near-net-shape manufacturing. However, there are several hurdles to large-scale commercial adoption of spray forming: 1) ensuring strip is consistently flat, 2) eliminating porosity, particularly at the deposit/substrate interface, and 3) improving material yield. Through this program, a new strip/sheet casting process, termed spray rolling, has been developed, which is an innovative manufacturing technique to produce aluminum net-shape products. Spray rolling combines the benefits of twin-roll casting and conventional spray forming, showing a promising potential to overcome the above hurdles associated with spray forming. Spray rolling requires less energy and generates less scrap than conventional processes and, consequently, enables the development of materials with lower environmental impacts in both processing and final products. Spray Rolling was developed as a collaborative project between the University of California-Davis, the Colorado School of Mines, the Idaho National Engineering and Environmental Laboratory, and an industry team.

Aluminum strip/sheet is manufactured commercially by conventional ingot metallurgical (I/M) processing and continuous casting (Lauener block casting, Hazelett belt, thin slab, twin roll, etc.). I/M processing remains the most reliable, versatile production method, accounting for about 70% of production in the U.S. However, it is energy and capital equipment intensive, reflecting the need to cast and homogenize ingots and hot work casting flaws. Ingots are direct-chill (DC) cast to about 20" thick, scalped, homogenized, hot rolled to about 0.2" thick re-roll stock, trimmed, and coiled. Following this, the coils are further processed (e.g. heat treated, cold rolled to final gauge, etc.) according to alloy composition and desired properties. Continuous casting of aluminum has seen significant growth over the past two decades, driven mainly by superior economics. One approach, twin-roll casting, combines solidification and hot rolling in a single operation. Liquid metal is fed into the gap between large water-cooled hollow rolls, where it solidifies to form strip up to about 0.25" thick. Twin-roll casting has long been viewed as an economic, streamlined strip-casting technology. Since its industrial inception about 50 years ago, the technology has improved steadily, particularly in the last twenty years. However, twin-roll casters usually operate much slower than the theoretical production-rate limit to satisfy quality requirements. And, due to production rate and quality issues, commercial sheet has been limited to alloys that have a suitably narrow freezing range.

Spray rolling consists of atomizing molten metal with a high velocity inert gas, extracting most of the metal's latent heat in-flight via convection cooling by entrained inert gas (to about 70% solid), and depositing the atomized droplets between mill rolls. The metal is consolidated into strip/sheet while still in a semi-solid and highly formable condition. As with twin-roll casting, it is believed that approximately 15% solid state compaction (hot rolling) occurs as the strip advances through the roll nip.

While spray rolling shares many similarities with twin-roll strip casting, there are important differences: (1) In twin-roll casting, the metal's latent heat is dissipated almost exclusively by conduction heat transfer to water-cooled rolls; (2) In spray rolling, convection heat transfer from small atomized droplets teams with conduction transfer at the rolls to increase the production rate

and limit segregation; and (3) The metal introduced to the rolls in twin-roll casting is molten, while in spray rolling, it has a semi-solid "slushy" character. Solid particles in the slush act as nucleation sites, producing an equiaxed grain structure and limiting segregation. Aluminum alloys with high alloy content and broad freezing ranges, such as 5083, 2124 and 7050, have been successfully spray rolled at comparatively high production rates.

Through the present study, 2124, 3003, 5083, 6111, and 7050 alloys were successfully processed into 100% dense, uniformly flat strip, thereby meeting critical project milestones. For all alloys, a refined microstructure was observed, with a uniform grain structure and uniform distribution of constituent particles. Using temper recipes supplied by industry, analysis of the spray-rolled strip indicated that mechanical properties were at least as good as those of commercial strip, while exhibiting a higher degree of isotropy. Production rates approximately 3X those of commercial twin-roll casters were demonstrated. These important findings demonstrated that spray rolling could eliminate energy-intensive DC casting, hot rolling and homogenization unit operations from commercial ingot-casting practices without sacrificing, and oftentimes improving, material properties due to rapid solidification.

Economic viability and environmental benefits associated with the use of spray rolling are significant. Estimated conversion costs for conventional ingot casting, continuous casting, spray rolling (10% overspray) and spray rolling (0% overspray) are $0.29, $0.28, $0.27, and $0.26 per pound of finished sheet, respectively [1]. Compared to ingot processing, cost savings for spray rolling are 13%, assuming 10% overspray. Annual projected savings for a facility with 1.05B lb./year capacity would be $45M. These savings do not take into account other potential cost savings opportunities such as the use of increased amounts of off-specification or recycled feedstocks above the limits which can be tolerated in conventional processing, the potential to use cheaper feedstock to produce equivalent properties, or the potential to design alloys with unique properties tailored to the process. Continued development and implementation of spray rolling will provide an energy efficient, low-cost strip-casting technology for the U.S. aluminum industry, and will likely lead to the development of unique alloys tailored to the process.

Spray rolling is environmentally friendly with negligible environmental impact. The process takes place inside closed chambers that are purged with nitrogen gas. During the process, molten metal is discharged into a high velocity jet of nitrogen. Nitrogen gas used during the process is filtered to remove airborne particulate prior to discharge to the atmosphere. Laser aerosol spectrometry measurements of particle concentration in the discharged gas indicated that the level is no higher than background, i.e., the HEPA filtration system is effective at removing essentially all airborne overspray. Spray rolling does not contribute to green house gas emissions. The environmental benefits of spray processing extend beyond the energy savings and limited scrap generation inherent to the process itself. The properties of the materials generated using these processes allow further benefits both in the following manufacturing steps and in the end use of these materials. The use of aluminum in automobiles can conserve huge quantities of petroleum because of improved fuel economies due to vehicle weight reduction [2]. Overall, lightweight/high strength materials could enable car manufacturers to design vehicles that would be 50-70% better fuel-efficient (30 to 50% lighter) without affecting safety, size or comfort [3].

Spray rolling can significantly reduce energy use during the processing of aluminum flat products. This is due to the elimination of DC casting, scalping, ingot homogenization, and hot

rolling unit operations in conventional ingot processing. In 2000, the U.S. aluminum industry produced 2,749,000 tons of hot rolled strip [4]. Potential energy savings are therefore about 23 x 10^{12} Btu (equivalent to 4 millions barrels of oil) annually. Additional (secondary) energy savings are possible if price reductions in the cost of sheet enabled greater use in automotive applications. The resultant improvements in fuel efficiency, and anticipated improvements in recyclability and tramp element tolerance of spray-rolled sheet, would result in even greater energy savings. For example, total energy requirements on a per-ton-finished-sheet basis are compared for conventional ingot casting, twin-roll casting and spray rolling (see Table 1). The energy penalty incurred in spray rolling due to overspray (0, 5, and 10%) is included in the table for comparison. In all cases, the energy required to process aluminum strip by spray rolling compares favorably with ingot processing. At 0% overspray, energy savings are 31%, which is very similar to twin-roll casting (32%), differing only by the energy required to cryogenically distill liquid air to obtain nitrogen gas used to atomize molten aluminum (an energy credit for the O_2 produced was included in the calculation). Data in Table 1 also underscores the importance of minimizing overspray during spray rolling, as the energy saved, compared to ingot processing, decreased from 31% to 25% to 19% as overspray increases from 0% to 5% to 10%, respectively.

Table 1. Energy Use and Energy Savings Per Ton Aluminum Sheet Produced by Ingot Casting, Twin-Roll Casting, and Spray Rolling.

Process	Energy Use, Btu (per ton finished sheet)	% Energy Savings (compared to ingot casting)
Conventional Ingot Casting	27.7×10^6	0%
Twin-Roll Casting	18.8×10^6	32%
Spray Rolling (0% overspray)	19.2×10^6	31%
Spray Rolling (5% overspray)	20.8×10^6	25%
Spray Rolling (10% overspray)	22.4×10^6	19%

II. Introduction

There exists a critical need for the transition from manufacturing technologies that require pollution disposal and remediation to technologies that allow pollution avoidance and energy savings while producing materials with superior combinations of microstructure and properties. As one such manufacturing method, net-shape manufacturing using spray forming has attracted considerable attention for the manufacture of aluminum alloys, reactive and high temperature materials. This technology is cost-effective, energetically economic and environmentally clean. The spray rolling process, which has been developed based on the spray forming technology, combines the benefits of spray forming and twin rolling to spray form strip/sheet materials suitable for near-net-shape manufacturing. This program has been successfully accomplished through expertise and facilities that have been developed at the University of California, the Colorado School of Mines, and the Idaho National Laboratory (formerly the Idaho National Engineering and Environmental Laboratory), in collaboration with an industrial team.

This program addresses two of the highest priority research needs of the "Finished Product Sector" (AITR, exhibit 4-5) as it contributes to (i) the understanding of the relationship of aluminum alloy composition and processing and its effect on microstructure and properties and (ii) the development of advanced forming and net-shape technology. These research needs as well as those related to the development and application of the computational and numerical methods to process design and simulation have been identified in the AITR amongst the research needs with the highest payoff for the "Finished Product Sector".

III. Background

Nearly all aluminum strip is manufactured commercially by conventional ingot metallurgical (I/M) processing, or continuous casting (Lauener block casting, Hazelett belt, thin slab, twin roll, etc.). I/M processing remains the most reliable, versatile production method, accounting for about 70% of domestic production. However, it is energy and capital equipment intensive, reflecting the need to hot work casting flaws. Ingots are direct chill cast to about 24" thick, scalped, homogenized, hot rolled to ~0.2" re-roll stock and coiled. Following this, the coils are coiled and further processed (e.g. precipitation hardened, cold rolled to final gauge, etc.) according to alloy and desired properties. Continuous casting of aluminum, driven mainly by superior economics, has seen significant growth over the past two decades, but mainly for niche markets with less demanding quality requirements.

Twin-roll casting, proposed originally by Bessemer [5], has long been viewed as the "Holy Grail" of strip casting. In this technique, liquid metal is fed into the gap between water cooled mill rolls, where it solidifies to form sheet. It combines solidification and hot rolling into a single operation. Aluminum twin-roll casters have seen limited commercial operation because historically these casters have had to run at a speed much lower than their theoretical limit to satisfy quality requirements. Current technical hurdles involve improving microstructural quality as well as improving process reliability and production rate. Structure defects can include banding of constituent phases, segregation, poor grain morphology and surface defects such as skulling, which arise due to nonuniform solidification. Side containment of the liquid pool, and uniform melt delivery to the nip of the rolls are the greatest engineering hurdles in twin roll casting [6-8].

Spray forming is a competitive low-cost alternative to ingot metallurgy (e.g., ingot casting, forging, and/or rolling) for the manufacturing of ferrous and non-ferrous alloy shapes. It produces materials of similar attractive combinations of properties but with a reduced number of processing steps and the possibility of near-net-shape manufacturing. Microstructure and property improvements have been reported for numerous spray deposited materials as compared to conventional materials; particularly interesting are those obtained for aluminum alloys, Cu alloys, Mg alloys, magnetic alloys, steels, Ni based alloys, Ti based alloys, and metal matrix composites [9]. In order to compete in the commercial marketplace against high-volume, established ingot metallurgy processes, other developments in spray forming have been made including [10, 11]:

- Spray forming of clad products;
- Spray forming of Al-Si alloy extrusion billets;
- Twin-atomizing technology for spray forming special steel billets up to 15.8 inch in diameter;
- Demonstration of low-cost manufacturing of superalloy ring;
- Construction of large pilot plants for spray forming of superalloys for turbine disks, and for copper alloy billets;
- Manufacture of bimetallic tubing.

Spray forming has shown its potential for the scale up to pilot plant for manufacturing of alloy tubing, rolls and billets. However, it has not been reported yet for the production of alloy strip/sheet by spray forming, in particular aluminum alloys. The main hurdles to successful commercialization of conventional spray forming are reducing porosity at the deposit/substrate interface, improving yield and ensuring a consistently flat strip profile during high volume production.

Spray rolling combines features of twin-roll casting and conventional spray forming. The proposed spray rolling approach should represent a processing improvement over conventional spray-forming approaches for strip production because it overcomes the main hurdles to large scale commercial adoption of spray forming: 1) ensuring strip is consistently flat, 2) elimination of porosity, particularly at the deposit/substrate interface, and 3) improving material yield. In the conventional spray forming approach, strip is produced by depositing metal droplets onto a plate or drum where it completely solidifies and is then thermomechanically processed. Strip must be sprayed flat (within about ±2.5%) to prevent fracture during subsequent rolling, a difficult engineering problem for large volume, continuous production. Rapid quenching of the droplets at the substrate results in an interconnected porosity band at the interface which can not be healed satisfactorily by rolling.

Spray rolling combines benefits of twin-roll casting and spray forming. It provides an increase in cooling rate of one to three orders of magnitude compared to twin-roll casting. Atomization increases the metal's surface area by a factor of about 10^{10}, thereby permitting substantial heat extraction rates in the spray with convection heat transfer coefficients in excess of 10^4 $Wm^{-2}K^{-1}$. During the process, semisolid material containing a very high concentration of grain refining nuclei is consolidated to full density. Compared with twin-roll casting, high solid fraction of the material delivered to the roll nip (~70%) in spray rolling will aid in providing a more uniform strip temperature during consolidation, producing a more homogeneous grain structure with very

limited segregation and constituent phase banding. It will also aid in side containment due to significantly higher viscosity of the semi-solid material. The higher costs associated with atomization should be balanced by the decreased need for subsequent hot work.

IV. Project Activities

The objectives of this project, achieved by the team, were:

(1) Demonstration of the feasibility of the spray rolling process at the bench-scale level and evaluation of the materials properties of spray rolled aluminum strip alloys;

(2) Demonstration of 2X scalability of the process and documentation of technical hurdles to further scale up and initiate technology transfer to industry for eventual commercialization of the process.

R&D activities accomplished by the team during the project are described below. The main technical accomplishments can be summarized as:

- Designed, constructed and tested the spray rolling strip caster.
- Verified process feasibility with 2124, 3003, 5083, 6111 and 7050 sheet alloys.
- Evaluated the influence of processing parameters on material properties, microstructure, production rate and yield.
- Analyzed microstructure of spray-rolled strip using optical microscopy, scanning electron microscopy (SEM), scanning transmission electron microscopy (STEM), energy dispersive spectroscopy (EDS), differential scanning calorimetry (DSC), X-ray diffraction, etc.
- Analyzed strip properties including ultimate tensile strength (UTS), yield strength (YS), elongation, hardness, thermal behavior, etc.
- Evaluated scale-up issues and demonstrated that the process is scalable by 2X.
- Characterization of the flow field induced by the spray in the spray-rolling chamber.
- Characterization of the polydispersed spray dynamics in the spray-rolling chamber.
- Evaluation of the enthalpy content and solid fraction in the spray along is trajectory.
- Parametric characterization of droplet impact, spreading and solidification (including influence on overspray).
- Evaluation of oxide volume fraction and dispersoid size distribution in the pre-rolled deposit using the integrated process model.
- Conducted modeling analysis of spray rolled geometry to determine when a transient state transits to a steady state during spray rolling.
- Developed a model to predict the maximum and minimum spray deposition rates during spray rolling for process control and continuous spray rolling operation.
- Developed a numerical model for analysis of thermal behavior and temperature during spray rolling.
- Investigated the formation of dispersoids during reactive atomization and deposition (RAD) as well as their effects on microstructures and mechanical properties of Al alloys.
- Developed a numerical model for analysis of evolution mechanism of grain size during spray forming.

- Carried out microstructural analysis of spray rolled 2124 Al strip using optical microscopy (OM) and transmission electron microscopy.

An overview of these accomplishments is given below. Additional technical details are available in the various publications listed in Part IV of this report.

4.1 Design and Construction of the Strip Caster

Photographs of the spray-rolling strip caster that was designed and constructed in the project are shown in Figure 1.

Figure 1: Photographs of the spray rolling strip caster.

The strip caster is comprised of a chamber that houses components to melt and atomize aluminum (Figures 1a and 1b), a conventional rolling mill (Figures 1a-d), a chamber to collect spray-rolled strips (Figure 1a), induction power units (Figure 1 b), and a gas manifold and system control panel (Figure 1e).

The square chamber shown in Figure 1a and 1b was adapted from a previous project and used to house induction coils, melt crucible, linear atomizer, and gas heater. Removable side walls permitted easy access to the spray forming components contained within. These components were mounted on an adjustable platform to help align the atomizers with the centerline of the rolls. An adjustable frame was constructed to support this chamber and help align it to the chamber housing the rolls. Caster wheels attached to the frame allowed the chamber to be rolled away from the rolling mill for easy access to spray forming components.

Spray forming components used to melt and atomize molten aluminum were designed and constructed in-house. These included:

- Pressurized melt crucible, molten metal flow control equipment, atomizer and gas heater.
- Induction coils to heat and melt aluminum, heat the atomizer, and heat the atomizing gas (nitrogen).
- Induction susceptors to couple the induction power to the melt crucible, atomizer and gas heater.

A chamber which encloses the rolling mill rolls was constructed and assembled. The enclosure is air tight, allowing the atmosphere within the spray rolling apparatus to be controlled to prevent

oxygen pick-up in the spray-rolled aluminum strip. Viewports in the enclosure were used for visual inspection of the spray impacting the rolls, and strips exiting the rolls via CCD cameras. Knife-edge strippers and strip guides were installed to aid detachment of the aluminum strip from the rolls and proper feeding of the strip into the collection chamber.

The rolling mill is a conventional Fenn 2-HI mill (Model 4-081) fitted with 8" diameter x 12" tool steel rolls that were not water cooled. The mill rolls were aligned to each other and positioned to coincide with the centerline axis of the spray nozzle. The electronics of the mill were modified to allow the surface speed of the rolls to be varied during operation. Diagnostics were added to monitor roll temperature, roll speed and roll gap, and to send input signals to digital readouts and a data acquisition system. In addition, equipment was constructed to apply lubrication to rolls during spray rolling.

A chamber and frame were constructed to collect the spray rolled strips. The chamber has a welded steel construction with several viewports for monitoring the quality of the spray-rolled strip exiting the rolls. A fold-down side panel provides access for removing strips. The chamber is mounted on a frame equipped with casters so that the chamber can be decoupled from the rolling mill enclosure. A two-stage filtration system was installed on the chamber to remove airborne particulate from the nitrogen gas stream discharged to the atmosphere.

Two induction-heating power units (Inductotherm Power-Trak, Model 75-30R) were utilized to melt metal, heat the atomizer, and heat atomizing gas. Modifications were made to the laboratory utilities (power and water) to support the power units. Insulated output leads and high-voltage chamber feedthroughs were installed.

A gas manifold was designed and assembled to monitor and control the flow of inert gas to various system components (atomizer, melt crucible, melt flow control equipment, and system purge). The manifold was mounted in a control panel that also houses the data acquisition system, readouts for pressure, temperature and flow, rolling mill controls, CCD camera monitors, and recorders. A screen splitter allows multiple images to be superimposed on a single screen. Video imaging equipment is used to monitor and record the spray impacting the rolls, strip exiting the rolls, and other views.

4.2 Production and Analysis of Spray-Rolled Strip

In a typical strip casting experiment, an aluminum alloy was induction melted under an inert gas atmosphere, superheated about $100^{O}C$ above the liquidus temperature, and atomized with nitrogen gas using a linear atomizer. An inert gas atmosphere within the spray apparatus minimized in- flight oxidation of the atomized droplets. Atomized droplets were deposited into the roll gap of the rolling mill operating at a roll surface speed of about 150 in./min., forming strip up to 8 in. wide and 0.062 in.- 0.25 in. thick. Since a coiler was not installed on the strip caster, individual 6 ft. long strips were formed by starting/stopping the spray. An example is shown in Figure 2.

Figure 2: As-spray rolled 2124 strip.

Strip production rates up to about 250 lbs/hr per inch strip width were demonstrated, with much higher production rates possible (with, for example, water-cooled rolls). These production rates compare favorably with commercial twin-roll casters, which operate at about 75 lbs/hr per inch strip width.

Industry partners selected 2124, 3003, 5083, and 7050 aluminum alloys for processing by spray rolling. In addition, 6111 alloy and three modified 5083 alloys were also supplied by industry participants for spray rolling trials. The wide range of compositions and melting rages of these alloys, summarized in Table 2, underscores the versatility of spray rolling.

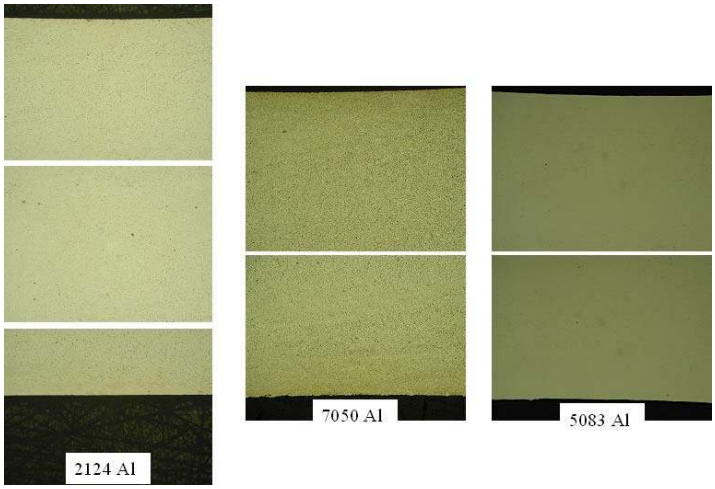

Figure 3: Cross sections of as-spray-rolled 2124 Al, 7050 Al, and 5083 Al.

Table 2. Nominal Composition and Melting Range of Aluminum Alloys Selected processed by spray rolling.

Alloy	Composition	Melting Range	Can alloy be twin-roll cast?	Can alloy be spray rolled?
2124	Al-4.4 Cu-1.5 Mg-0.6 Mn	502 – 638°C	No	Yes
3003	Al-1.2 Mn-0.12 Cu	643 – 654°C	Yes	Yes
5083	Al-4.4 Mg-0.7 Mn-0.15 Cr	574 – 638°C	No	Yes
6111	Al-0.9 Si-0.7 Cu-0.75 Mg-0.3 Mn	587 – 650°C	No	Yes
7050	Al-6.2 Zn-2.3 Cu-2.3 Mg-0.12 Zr	524 – 635°C	No	Yes

As-spray-rolled strip was characterized by a flat, uniformly thick profile, with no porosity and minimal segregation. Figure 3 illustrates the uniform microstructure that was obtained in transverse cross section. The grain structure was equiaxed, with a typical average grain size of about 10 μm. Figure 4 compares the microstructure of ingot-cast 2124 (Figure 4a) with as-spray-rolled 2124 (Figure 4b), commercial 2124-T85 material (Figure 4c) and spray-rolled 2124-T85

strip (Figure 4d). Extensive segregation and shrinkage voids characterized the ingot-cast material. Commercially, the material is homogenized at high temperature for an extended period to reduce interdendritic segregation and solutionize precipitates that form during casting. It is then extensively hot worked to break-up and redistribute the segregate. In contrast, the as-spray-rolled 2124 is characterized by a fine-grained equiaxed structure with relatively small constituents. Following solution heat treatment and aging to a T85 temper, both the spray-rolled and ingot-processed 2124 exhibit a recrystallized grain structure. However, the anisotropy of the grain structure is quite different. The commercial material has highly elongated grains (Figure 4c) while the grains of the spray-rolled material are nearly equiaxed due to the relatively modest amount of rolling during processing. As a result, tensile tests demonstrated that the mechanical properties of the spray-rolled 2124 were more isotropic than commercial material.

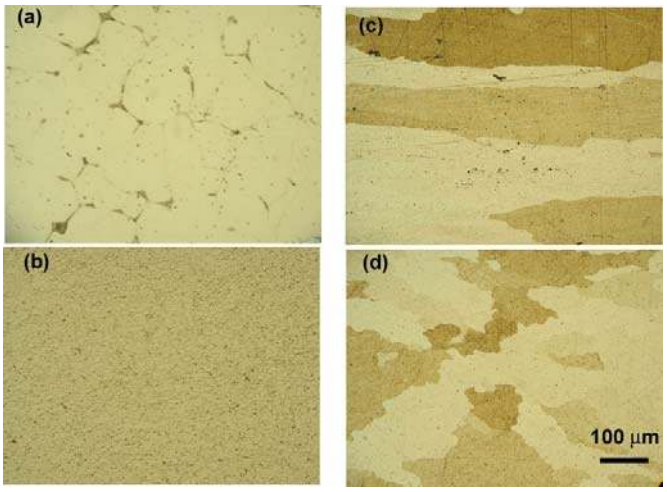

Figure 4: Photomicrographs of 2124 Al. (a) Ingot cast, (b) as-spray rolled, (c) commercial plate (T85), and (d) spray rolled-T85. Keller's etch.

Extensive microstructure/property analysis was performed on the spray-rolled alloys listed in Table 2. Microstructure was evaluated using an Olympus Model PME-3 metallograph and a Philips XL-30 ESEM scanning electron microscope. Tensile testing was performed with an Instron 4505 screw-driven test machine following the ASTM E-8 procedure. Differential thermal analysis was performed with a Rheometrics Model DTA 1500 using a scan rate of 20^{O}C/min. For STEM analysis, thin slabs, 0.020-0.030 in. thick, were cut from samples of spray-rolled and commercial material and ground using silicon carbide paper until they were approximately 0.010 in. thick. 0.118 in. diameter TEM blanks, were punched from each thinned slab and electropolished at 25 volts to perforation using a solution of ethanol-5% perchloric acid held at approximately -10^{o}C. The electropolished samples were rinsed with ethanol and examined using a Philips EM401 Scanning Transmission Electron Microscope in the STEM mode at 120 KV. X-ray diffraction was performed using Cu (Kα1 + Kα2) radiation on a Bruker Model D-8 Advance system operating at a sampling rate 0.6° (2 theta) per minute. Resulting patterns were analyzed with EVA software.

3003 and 5083 Al Alloys

The non-heat-treatable aluminum alloys 3003 and 5083 were selected by industry partners for processing by spray rolling. 3003 alloy is manufactured commercially by I/M processing and continuous casting, including twin-roll casting. In contrast, 5083 alloy has seen very limited commercial production via twin-roll casting, largely due to its high Mg content (4.4 wt. %) and broad freezing range, which reduce production rate and quality. When processed by spray rolling, 3003 alloy was found to be less sensitive to the liquid fraction of the spray at impact with the rolls than was 5083 alloy. One problem encountered with 3003 alloy, however, that was not encountered with 5083 was the tendency for the strip to stick to the rolls. This tendency increased as the strip thickness decreased, and as the load applied to the rolls increased. There was no tendency for 3003 strip to stick to the rolls unless a load was applied to the strip during hot deformation in the roll nip. Sticking, which appears to be analogous to soldering in die casting, is overcome by applying a thin layer of graphite or other solid lubricant to the rolls. Similar sticking behavior is also observed in twin-roll casting.

3003 and 5083 strips were produced measuring 4 in. wide x 0.15 in. thick at a rate of 125 lb/h-in. Strips measuring 8 in. wide x 0.15 in. thick were also produced at 125 lb/h-in by decreasing the roll speed and allowing the semisolid material to flow laterally. Prior to tensile testing and microstructure analysis, these samples were processed using the following recipes:

- Spray rolled → annealed (530°C, 1 h)
- Spray rolled → annealed (530°C, 10 min) → cold rolled 35%
- Spray rolled → annealed (530°C, 30 min) → cold rolled 35%
- Spray rolled → annealed (530°C, 1 h) → cold rolled 35%
- Spray rolled → annealed (530°C, 2 h) → cold rolled 35%
- Spray rolled → annealed (530°C, 3 h) → cold rolled 35%
- Spray rolled → annealed (530°C, 1 h) → cold rolled 10%
- Spray rolled → annealed (530°C, 1 h) → cold rolled 20%
- Spray rolled → annealed (530°C, 1 h) → cold rolled 35%
- Spray rolled → annealed (530°C, 1 h) → cold rolled 55%
- Spray rolled → annealed (530°C, 1 h) → cold rolled 75%

The influence of time at temperature on annealed samples was evaluated by heating samples for 10 min., 30 min., 1, 2, and 3 h. Strips of 3003 aluminum alloy that were heated for 1 h and cold rolled to 35%, 55%, and 75% thickness reduction simulated commercial H14, H16, and H18 tempers, respectively.

Tensile results are summarized in Table 3. For comparison, typical values and minimum specification limits for commercial sheet of comparable gauge are included. As can be seen from Table 3, spray-rolled tensile properties compare favorably with those of commercial sheet. Most notably, for a given elongation, the strength of spray-rolled 3003 is about 30% higher. This is attributable to its finer grain size and constituent particle size. Samples were also annealed at 430°C. However, it was found that the higher annealing temperature (530°C) provided a better combination of tensile properties, presumably because it allowed for some redistribution of solute-rich phases and more thorough removal of strain hardening during spray rolling. However, as shown in Table 3, soak times longer than 10 min did not significantly influence tensile properties. The tensile properties of 8 in. wide 3003 strips were similar to those of 4 in. wide

thick strips. In addition, no significant variation in properties was noted along the length or width of strip. Transverse and longitudinal properties were similar.

Table 3. Tensile properties of 3003 Al alloy sheet. Commercial values are typical, with minimum specification values in parenthesis.

Condition	Ultimate Tensile Strength (ksi)	Yield Strength (ksi)	Elong. (%)
Commercial O	16 (14)	6 (5)	30 (25)
Commercial H14	22 (20)	21 (17)	8 (5)
Commercial H16	25 (24)	25 (21)	5 (4)
Commercial H18	29 (27)	27 (24)	4 (3)
As spray rolled	23	16	19
Spray rolled, annealed (530°C, 1 h)	21	12	34
Spray rolled, annealed (530°C, 10 min.), cold rolled 35%	29	27	7
Spray rolled, annealed (530°C, 30 min.), cold rolled 35%	29	29	7
Spray rolled, annealed (530°C, 1 h), cold rolled 35%	30	28	8
Spray rolled, annealed (530°C, 2 h), cold rolled 35%	30	29	7
Spray rolled, annealed (530°C, 3 h), cold rolled 35%	29	29	8
Spray rolled, annealed (530°C, 1 h), cold rolled 10%	23	20	24
Spray rolled, annealed (530°C, 1 h), cold rolled 20%	27	26	14
Spray rolled, annealed (530°C, 1 h), cold rolled 35%	30	28	8
Spray rolled, annealed (530°C, 1 h), cold rolled 55%	33	31	7
Spray rolled, annealed (530°C, 1 h), cold rolled 75%	38	36	6

Figure 5 compares the morphology and distribution of primary constituent particles in spray-rolled/annealed and commercial 3003 sheets. Somewhat finer constituent particle sizes were found near the surface of spray-rolled strip than in the middle due to a higher cooling rate at the surface. Constituents near the surface were also rounder, while those in the middle were more elongated and tended to follow the contour of grain boundaries. Coarse sprays with high liquid fraction favored the formation of fewer, but larger, constituent particles.

Compared to 3003 alloy, processing 5083 alloy required closer control of the solid fraction of the slush introduced to the rolls. If the solid fraction was suitably high, a uniform microstructure was obtained, as shown in Figure 3. A high liquid fraction resulted in the solute-rich phase being squeezed to the surface. Figure 6a illustrates surface segregation in spray-rolled 5083 formed under high-liquid-fraction conditions. Energy dispersive spectroscopic (EDS) analysis of the surface (Figure 7) indicated that the segregate was enriched in Fe and Mn (spot A in Figure 7a), and had a composition similar to the principal constituent phases in commercial sheet, $(Mn,Fe)Al_6$. $(Mn,Fe)_3SiAl_{12}$, constituent particles and smaller amounts of Mg_2Si, was also observed. The EDS element maps of Figure 8 further show the distribution of Al, Mg, Mn, Fe,

and Cr in the vicinity of the surface segregate. K-line transition signals were accumulated for about 1 h to generate the maps.

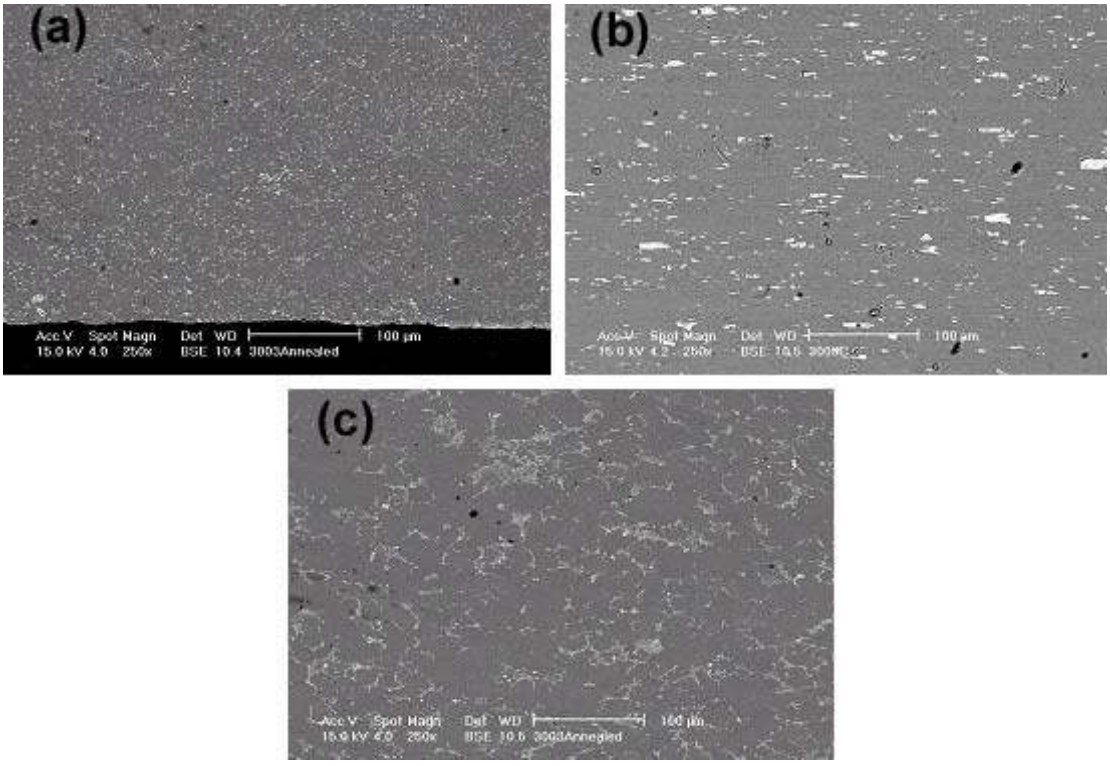

Figure 5: SEM photomicrographs (backscattered electron mode) showing constituent particle distributions in spray-rolled/annealed and commercial 3003 Al sheet. (a) Spray-rolled/annealed, strip edge. (b) Commercial 3003-H14 sheet. (c) Spray-rolled/annealed, strip center. As-polished.

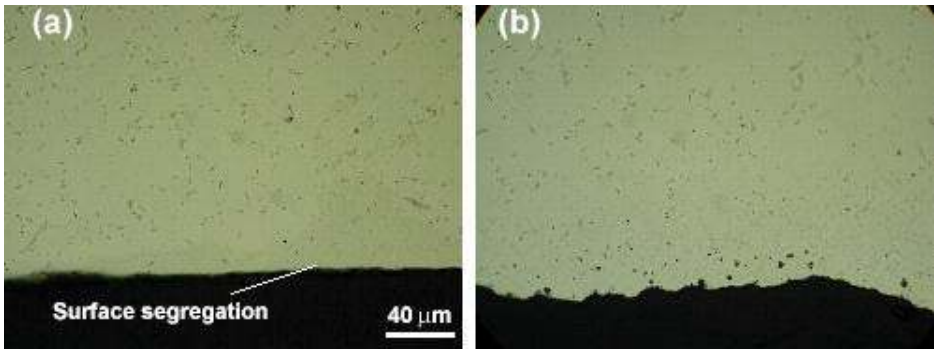

Figure 6: Spray-rolled 5083 processed with an unacceptably high fraction of liquid in the spray. (a) As spray rolled. (b) Diffusion resulted in surface defects after heating at 530°C for several hours

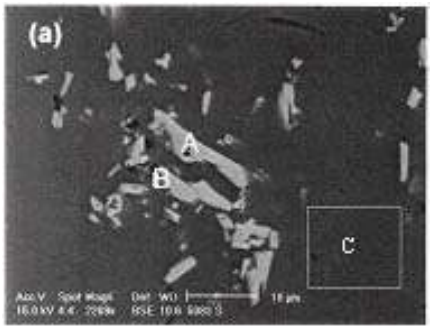

Element	Spot A (wt.%)	Spot B (wt.%)	Spot C (wt%)
Mg	0.5	7.1	3.9
Mn	17.2	9.0	1.0
Si	0	3.7	0.2
Fe	15.0	8.9	0.1
Al	67.3	71.4	94.9

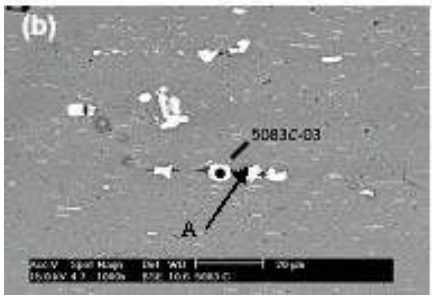

Element	Spot A (wt.%)
Mg	0
Mn	17.4
Si	1.4
Fe	14.8
Al	66.4

Figure 7: SEM photomicrographs (backscattered electron mode) of 5083 Al. (a) Surface of spray-rolled material of Figure 6a. (b) Commercial sheet. Tables give EDS composition analysis of features.

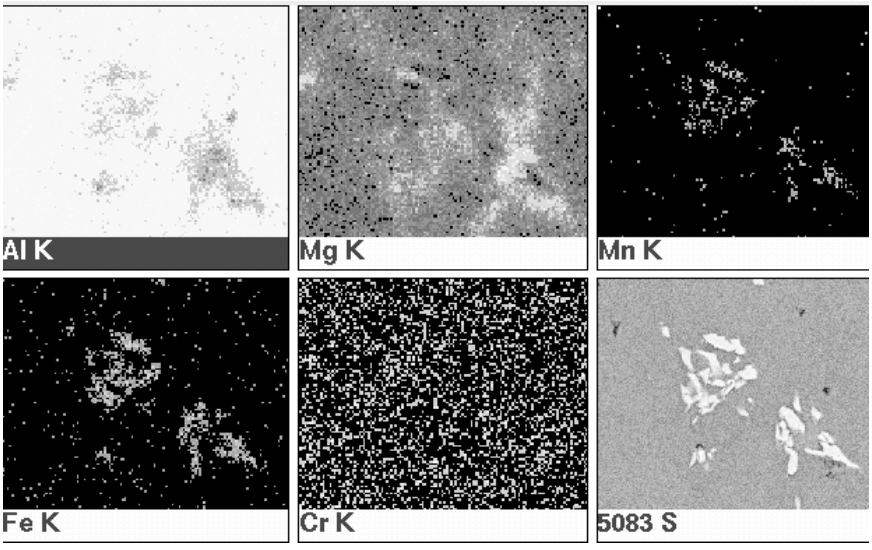

Figure 8: EDS element maps of spray-rolled 5083 Al near surface segregation of Figure 6a. An SEM image of the region is shown in the lower right. Light colored areas indicate element concentrations.

Heating the spray-rolled 5083 strips at 530°C caused the solute-rich phase to diffuse into the matrix. However, this diffusion was accompanied by the formation of surface pitting, as illustrated in Figure 6b (Kirkendall diffusion).

Low-liquid-fraction processing conditions eliminated localized surface segregation in 5083 and resulted in strip with favorable mechanical properties. Strip was annealed using the following recipes:

- Spray rolled → annealed (530°C, 10 min)
- Spray rolled → annealed (530°C, 30 min)
- Spray rolled → annealed (530°C, 1 h)
- Spray rolled → annealed (530°C, 2 h)
- Spray rolled → annealed (530°C, 4 h)
- Spray rolled → annealed (530°C, 8 h)

Results of the tensile analysis are summarized in Table 4. Typical values and minimum specification limits for fully-annealed commercial sheet of comparable gauge are included. As shown in Table 4, strip annealed at 530°C for 30 min or longer provided elongation values that compare favorably with those of commercial sheet. In contrast to spray-rolled 3003 strip, spray-rolled 5083 appeared to benefit from extended heating at 530°C, which improved elongation.

Table 4. Tensile properties of 5083 Al alloy sheet. Commercial values are typical, with minimum specification values in parenthesis.

Condition	Ultimate Tensile Strength (ksi)	Yield Strength (ksi)	Elongation at Failure (%)
Commercial, annealed (O temper)	42 (40)	21 (18)	22 (16)
As spray rolled	40	32	8
Spray rolled, annealed (530°C, 10 min.)	38	19	20
Spray rolled, annealed (530°C, 30 min.)	43	19	30
Spray rolled, annealed (530°C, 1 h)	44	18	31
Spray rolled, annealed (530°C, 2 h)	43	19	34
Spray rolled, annealed (530°C, 4 h)	44	19	34
Spray rolled, annealed (530°C, 8 h)	44	20	37

2124 and 7050 Al Alloys

Industry participants selected two heat-treatable aluminum alloys, AA2124 and AA7050, for extensive processing by spray rolling. These aerospace alloys have high alloy content and broad freezing ranges, making them difficult to process commercially, even by the conventional ingot/metallurgical (I/M) method. Currently, they are not strip cast commercially due to their broad freezing ranges.

Processing these alloys by spray rolling did not present any significant technical difficulties. 2124 alloy did have a tendency to stick to unlubricated rolls, particularly under high load conditions. The application of a lubricant to the rolls was beneficial. With 7050 alloy, care

needed to be exercised to ensure that the melt superheat temperature was not excessive, as the combination of high equilibrium vapor pressure of zinc (about 100 torr at 750°C) together with the large increase in melt surface area during atomization, could lead to zinc depletion. Chemistry analysis of the starting material and as-spray-rolled strip indicated that no change in chemistry occurred for either alloy during processing.

Prior to tensile testing, as-spray-rolled strip was edge trimmed. Both commercial and spray-rolled 2124 strip were heat treated to the T85 and T851 tempers, with cold rolling substituted for the normal commercial practice of stretching. Annealing was performed by heating strip to 413°C, soaking for 5 min to 24h, cooling at 25 °C/h to 232°C, holding at temperature for 4h, followed by slow cooling in the furnace.

The following recipes were used:

- Solution treated (493°C, 1 h) → water quenched→ aged (190°C, 12 h)
- Solution treated (493°C, 1 h) → water quenched→ cold rolled 5%→ aged (190°C, 12 h).
- Solution treated (493°C, 2h) → water quenched→ cold rolled 3%→ aged (190°C, 12 h).
- Solution treated (493°C, 2h) → water quenched→ cold rolled 10%→ aged (190°C, 12 h).
- Annealed using the standard industry practice for the alloy.

Table 5. Tensile properties of 2124 Al.

Material and Heat Treatment*	Ultimate Tensile Strength (ksi)	Yield Strength (ksi)	Elongation at Failure (%)
Commercial 2124 –T851	62	57	4
As spray rolled 2124	46	38	10
SR 2124-ST (1 hr.)-A	66	52	7
COMM 2124- ST (1 hr.)-A	63	55	6
SR 2124-ST (1 hr.)-CR 5%-A	74	70	4
COMM 2124- ST (1 hr.)-CR 5%-A	70	68	3
SR 2124-ST (2 hr.)-CR 3%-A	70	68	7
COMM 2124-ST (2 hr.)-CR 3%-A	68	66	2
SR 2124-ST (2 hr.)-CR 10%-A	74	69	5
COMM 2124-ST (2 hr.)-CR 10%-A	70	68	2
SR2124-ANN	28	17	15
COMM-ANN	27	12	19

*SR is spray rolled, ST is solution treated (493^{O}C), CR is cold rolled, A is artificially aged (190^{O}C, 12 hrs.), ANN is annealed (348^{O}C, 2 h + 232 ^{O}C, 4 h).

To help ensure equivalence when comparing tensile properties, commercial plate was machined to the same thickness as the spray-rolled strip, and was solution heat treated, cold rolled, precipitation hardened, and tensile tested side-by-side with spray-rolled strip. Similarly, commercial and spray-rolled samples were annealed side-by-side in a furnace.

Tensile results for 2124 Al, summarized in Table 5, indicated that spray-rolled strip tensile properties compare favorably to those of commercial I/M strip with the same temper. Moreover, tensile properties of spray-rolled material appear to be less sensitive to rolling direction, because the amount of rolling is very small compared to I/M processing.

Consistent improvement in the tensile properties of spray-rolled strip over commercial strip followed inclusion of a cold rolling step in the heat treatment recipes. Spray-rolled strip also appeared to benefit from a somewhat longer heat treatment period than did the commercial strip. Annealed spray-rolled 2124 had lower ductility but higher yield strength than commercial 2124, suggesting that the commercial recipe that was followed should be modified somewhat to increase ductility for the spray-rolled alloy, if desired.

STEM analysis was performed on commercial 2124-T851 plate, as-spray-rolled 2124 strip, and spray-rolled 2124-T851 strip. Representative STEM images are shown in Figure 9. The commercial material and spray-rolled 2124-T851 were nearly identical. Both exhibited very large grains (also see Figure 4) that exceeded the electron transparent area. Large (>300 nm) manganese-containing precipitates, and much finer (<50 nm) round precipitates were observed in both samples. In contrast, the as-spray-rolled sample was characterized by very fine (1-10 μm) grains and fewer of the large manganese-containing precipitates than was found in the heat treated samples. The as-spray-rolled 2124 strip also had a relatively high dislocation density indicating that the strip experiences some degree of cold work during spray rolling.

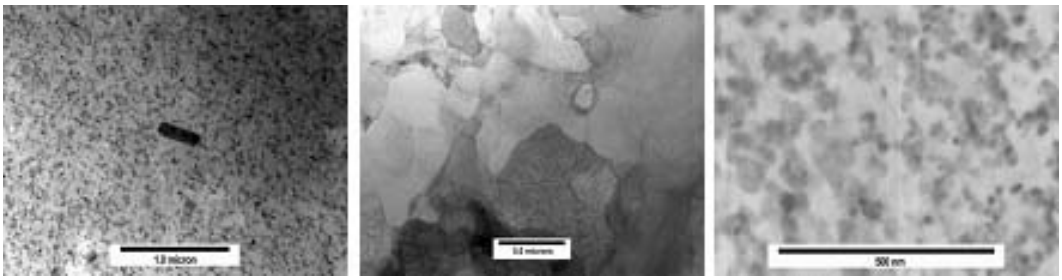

Figure 9: STEM photomicrographs of commercial 2124-T851 plate (left), as-spray-rolled 2124 (center), and spray-rolled 2124-T851 strip (right).

Energy dispersive spectroscopic (EDS) element maps of commercial 2124 plate and as-spray-rolled 2124 are shown in Figure 10. These maps show the distribution of Al, Cu, Mg, Fe, and Mn in the primary constituent phase and surrounding matrix. K-line transition signals were accumulated for about 1 h to generate the maps. In these maps, light colored areas indicate the presence of that particular element, while dark areas indicate the absence of the element. The main constituent phase of the commercial 2124 plate is found to be enriched in Cu, Fe and Mn relative to the surrounding matrix, which is enriched in Al and Mg. The primary constituent phase in as-spray-rolled 2124 is found to be enriched in Cu, depleted in Al, with Mg, Fe, and Mn uniformly distributed in the matrix and constituent phases.

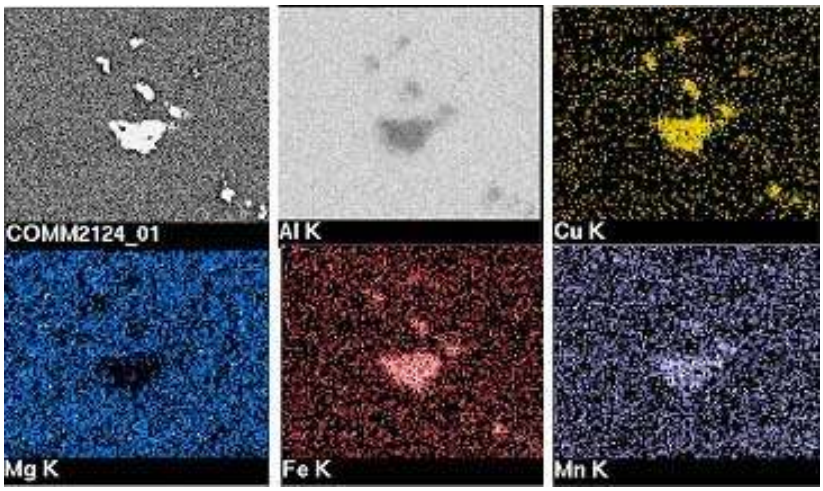

(a)

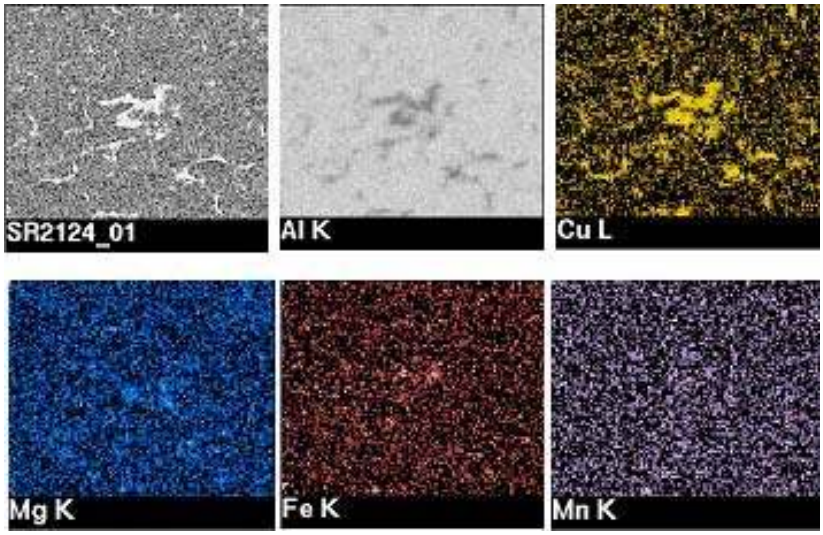

(b)

Figure 10: EDS element maps of (a) commercial 2124 plate, and (b) spray-rolled 2124 strip.

X-ray diffraction analysis of as-spray-rolled 2124, spray-rolled 2124-T851 and commercial 2124-T851 are summarized in Figure 11. Scan profiles of both 2124-T851 strips were similar. Primary Al peaks in the as-spray-rolled 2124 scan were shifted somewhat due to lattice strain, and show more clearly resolved peaks corresponding to Al_2CuMg and Al_2Cu constituent phases.

When processed by spray rolling, the properties of 2124 alloy were found to be sensitive to the solid fraction of the spray when it impacts the rolls. Solid fraction can be controlled by adjusting the amount of gas that mixes with the molten metal in the atomization zone, the gas–to-metal mass flow ratio (G/M). G/M influences average droplet size in the spray, and consequently, droplet cooling rate. Strip samples produced at G/M values of 0.15 and 0.30 showed marked differences in constituent particle size and distribution and resultant tensile properties in both the as-spray-rolled and T851 temper states. The production rate for strip samples was 250 lb/h-in.

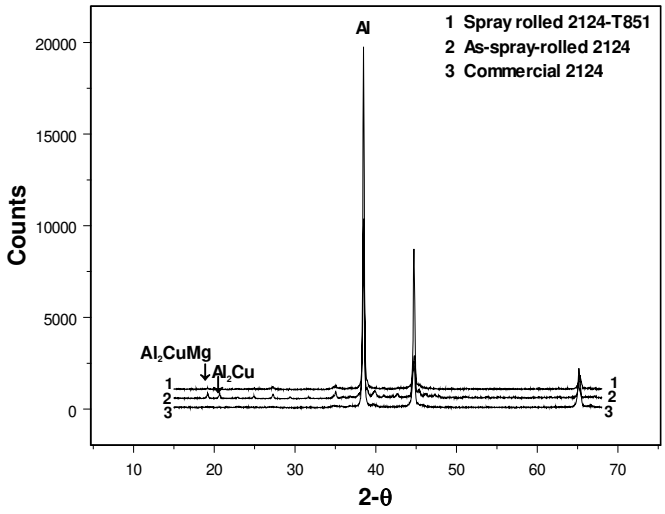

Figure 11: X-ray diffraction scans of as-spray-rolled 2124, spray-rolled 2124-T851 and commercial 2124-T851.

Figure 12 compares the microstructure of cast 2124 with as-spray-rolled strips produced at two G/M values. The cast material is characterized by a coarse dendritic structure and extensive interdendritic segregation of the solute-rich phases. In contrast, spray-rolled material exhibited a fine-grain size (about 10 μm), nearly equiaxed structure with relatively small Al_2CuMg and Al_2Cu constituents. The material produced at G/M = 0.15 had a somewhat larger average grain size, with larger and more numerous constituent particles, particularly near the surface of the strip. This was due to the solute-rich phase being squeezed to the surface during compaction in the roll gap.

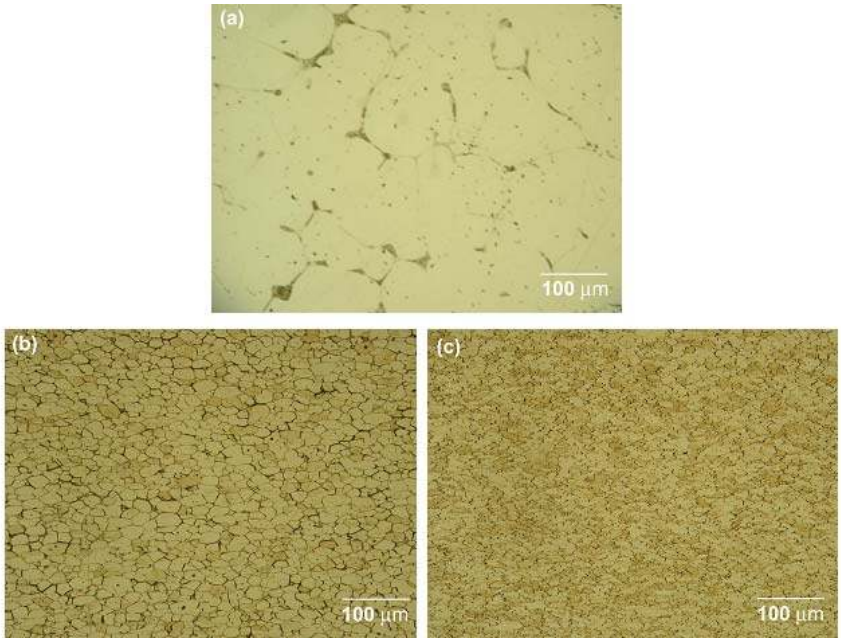

Figure 12: Photomicrographs of 2124 aluminum. (a) Cast. (b) As-spray-rolled using G/M = 0.15. (c) As-spray-rolled using G/M = 0.30.

Tempering spray-rolled 2124 to the T851 condition resulted in a recrystallized grain structure with some spheroidization of constituents. The microstructure of longitudinal sections of strip samples produced at G/M = 0.15 and 0.30 was similar in terms of grain size and morphology (Figure 13a and 13b), with relatively little grain elongation compared to commercial 2124 (Figure 13c) due to the modest amount of rolling during processing. Moreover, tensile properties of transverse and longitudinal sections cut from spray-rolled strip are very nearly identical, in contrast to commercial material.

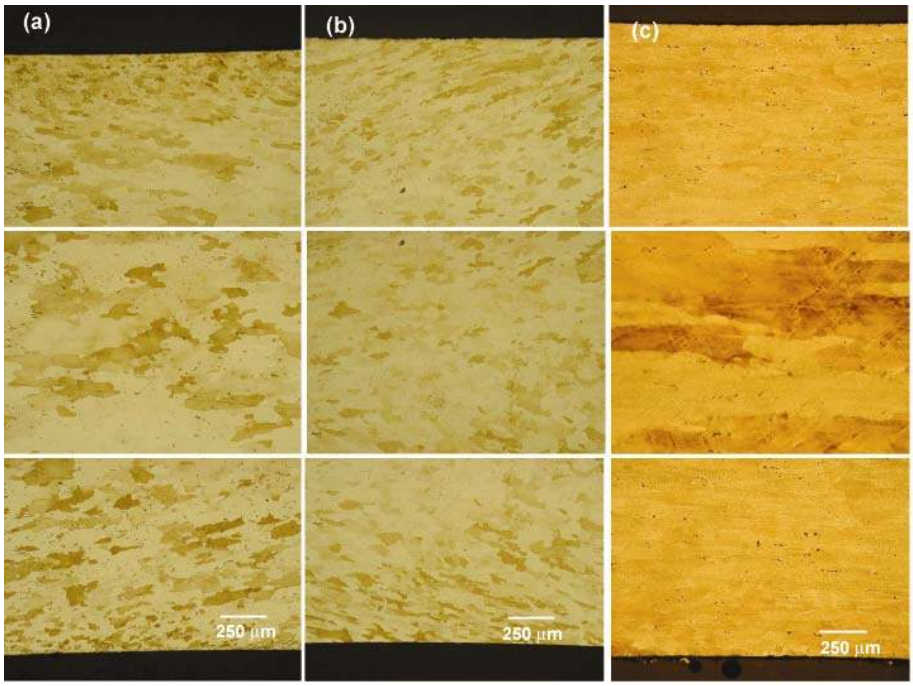

Figure 13: Longitudinal photomicrographs of 2124-T851 aluminum. (a) Spray rolled at G/M = 0.15 near each rolling surface (top, bottom) and near the center of a 4.3 mm thick strip. (b) Same as (a) but spray rolled at G/M = 0.3. (c) Commercial plate near each rolling surface (top, bottom) and near the center.

Tensile properties of as-spray-rolled 2124 strip and 2124-T851 strip processed at G/M=0.15 and 0.30 are summarized in Table 6. Results indicate that increasing the solid fraction of the "slush" introduced into the roll gap by increasing G/M improves tensile properties. For as-spray-rolled 2124 strip, increasing G/M from 0.15 to 0.30 resulted in an increase in UTS of 39%, an increase in YS of 46% and a doubling of the ductility. This is largely due to a reduction in segregation, particularly at the strip surface, and more uniform distribution of constituent phases at G/M = 0.30. This trend was also observed following tempering to the T851 condition. Increasing G/M from 0.15 to 0.30 resulted in an increase in UTS, YS and % elongation of 9%, 15%, and 17%, respectively. As shown in Table 6, the tensile properties of 2124-T851 produced at G/M = 0.30 compare favorably with those of commercial material.

Table 6. Tensile properties of as-spray-rolled 2124 and 2124-T851.

Condition	G/M	Ultimate Tensile Strength (ksi)	Yield Strength (ksi)	Elongation at Failure (%)
Commercial-T851	-	70	65	6
As spray rolled	0.15	33	26	5
As spray rolled	0.30	46	38	10
Spray rolled –T851	0.15	64	59	6
Spray rolled –T851	0.30	70	68	7

Table 7 summarizes tensile properties of spray-rolled and annealed 2124 produced at G/M = 0.15. Annealing was performed by heating strip to 413°C, soaking for 5 min to 24h, cooling at 25°C/h to 232°C, holding at temperature for 4h, followed by slow cooling in the furnace.

Table 7. Tensile properties of annealed 2124. Spray-rolled strip was processed at G/M = 0.15.

Sample/Soak time at 413°C	Ultimate Tensile Strength (ksi)	Yield Strength (ksi)	Elongation at Failure* (%)
Commercial	27	11	20
Spray rolled/ 5 min.	27	13	16
Spray rolled/ 30 min.	29	14	17
Spray rolled/ 1 h.	30	14	18
Spray rolled/ 2 h.	29	14	15
Spray rolled/ 4 h.	29	14	16
Spray rolled/ 8 h.	29	15	15
Spray rolled/ 16 h.	29	14	16
Spray rolled/ 24h.	29	15	18

*The minimum specification for elongation at failure is 12%

Optimal properties were obtained following a soak at 413°C for a period of about 1 h. Compared to commercial 2124, the yield strength of spray-rolled 2124 was higher and the ductility somewhat lower, suggesting the commercial practice for annealing 2124 may not be optimized for spray-rolled 2124.

Spray-rolled 7050 alloy was heat treated to simulate the T76 and T7651 tempers using the following recipes, with 3% cold rolling substituted for the normal commercial practice of 3% stretching:

- Solution treated (471°C, 2-15 h) → water quenched→ aged (125°C, 12 h + 166°C, 15 h).
- Solution treated (471°C, 2-15 h) → water quenched→ cold rolled 3%→ aged (125°C, 12 h + 166°C, 15 h).

DTA analysis was performed on samples of solution heat treated (471^{O}C soak for 2 hours) commercial plate and spray-rolled strip, in addition to as-spray-rolled 7050. DTA is useful for analyzing heat absorption or heat evolution that accompanies phase transformations, precipitation of new phases, resolution of phases, etc. Scan data and peak assignments are summarized in Figure 14. The scans for both solution heat treated samples were very similar.

Peaks corresponding to the exothermic precipitation of phases at low temperature during aging were observed for both solution treated samples but not the as-spray-rolled 7050 strip. In addition, a small endothermic peak, assigned to the melting of nonequilibrium eutectic was seen for the as-spray-rolled 7050.

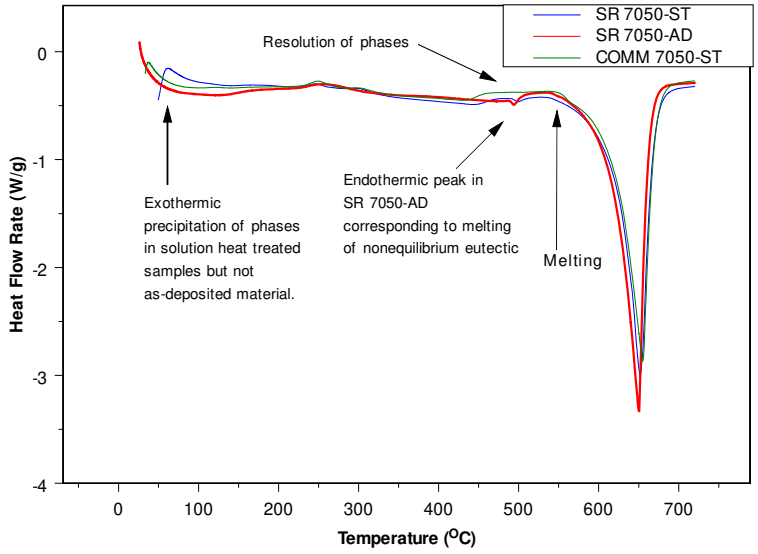

Figure 14: Differential Thermal Analysis scans on spray-rolled and commercial 7050 aluminum alloy samples.

Table 8. Tensile properties of spray-rolled and commercial 7050 aluminum strip.

Material and Heat Treatment*	Ultimate Tensile Strength (ksi)	Yield Strength (ksi)	Elongation at Failure (%)
Commercial 7050-T7651 plate	74	65	12
As spray rolled 7050	58	43	14
SR 7050-ST (2 h) - A	79	72	10
SR 7050-ST (5 h) - A	76	67	10
SR 7050-ST (10 h) - A	78	71	10
SR 7050-ST (15 h) - A	79	73	7
SR 7050-ST (2 h)-CR 3%-A	72	64	8
SR 7050-ST (5 h)-CR 3%-A	77	69	10
SR 7050-ST (10 h)-CR 3%-A	75	66	10
SR 7050-ST (15 h)-CR 3%-A	75	66	10

*SR is spray rolled, ST is solution treated (471°C), CR is cold rolled, A is aged (125°C, 12 h + 166°C, 15 h).

The latter observation suggested that the length of time used in normal commercial practices to solution heat treat homogenized and hot rolled sheet may not be appropriate for the as-spray-rolled material. To evaluate this, samples were soaked at 471^{O}C for 2, 5, 10, and 15 h, water quenched, and aged (125°C, 12 h + 166°C, 15 h). Additional samples were cold rolled 3% after solution treatment, and aged. Tensile test results conducted on these samples are summarized in Table 8. For comparison, tensile results for commercial 7050-T7651 plate are included. To help ensure equivalence when comparing tensile properties, commercial plate was machined to the

same thickness as the spray-rolled strip, and tensile tested at the same time as spray-rolled strip. Results indicate that the overall properties of the spray rolled and heat treated 7050 are similar to those of the commercial material. 3% cold reduction of the spray-rolled 7050 resulted in a small decrease in strength compared with material that was not cold rolled. This is likely due to coarsening of η' precipitates that form along dislocations during aging.

Figure 15 compares the microstructure of 7050 in the cast, as-spray-rolled and heat treated conditions. Interdendritic segregation, coarse constituents, and shrinkage voids were found in the cast material (Figure 15a) that formed during slow cooling of the alloy. As with 2124 alloy, the as-spray-rolled 7050 is characterized by a fine-grained (about 10 μm) equiaxed structure with relatively small constituents that tend to be located along grain boundaries (Figure 15b). Following solution heat treatment, stretching and aging to a T7651 temper, the recrystallized microstructure of the commercial 7050 appears as in Figure 15c, when viewed in the longitudinal direction. Spray rolled 7050-T76 has a similar microstructure to that of the commercial material except that the recrystallized grains do not show nearly the directionality due to the relatively modest amount of rolling during processing. Also, constituents tend to be more randomly distributed and somewhat finer than in the commercial plate.

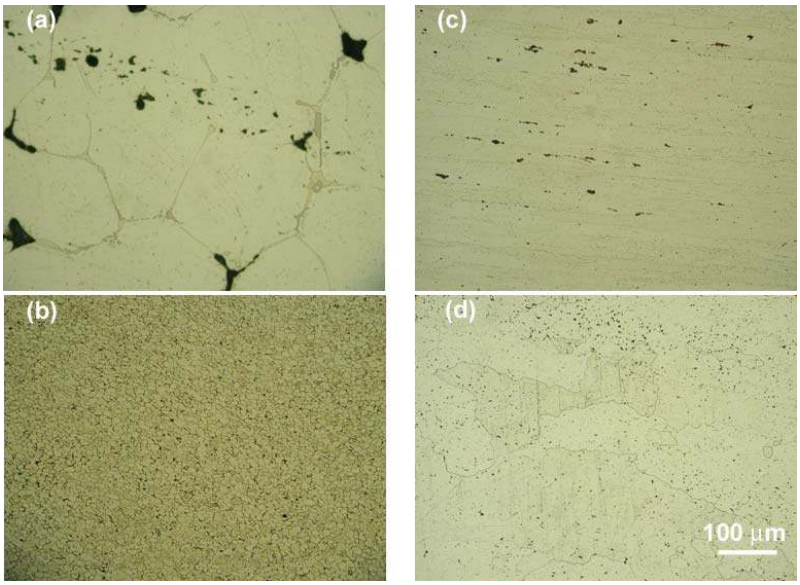

Figure 15: Photomicrographs of 7050 Al. (a) Ingot cast, (b) as-spray-rolled, (c) commercial 7050-T7651 plate, (d) spray rolled 7050-T76. The SEM photomicrographs of Figure 16 compare the morphology and distribution of primary constituent particles in as-spray-rolled and commercial 7050 sheets. EDS analysis of the constituents (light phase) and surrounding matrix (dark phase) is summarized in the tables accompanying the photomicrographs. The tendency for constituent phases in the commercial material to be aligned in the direction of hot rolling was not observed with spray-rolled strip. The as-spray-rolled and commercial 7050 materials showed some variation in the relative composition of constituent and matrix phases. In particular, the constituents in the commercial material were particularly enriched in Fe and Cu while those in the as-spray-rolled 7050 were enriched in Cu, Mg, and Zn.

Element	Light Phase wt.%	Dark Phase wt.%
Al	63.34	90.13
Cu	24.54	1.77
Mg	1.14	2.74
Zr	0.05	0.08
Zn	0.21	5.20
Fe	10.72	0.08

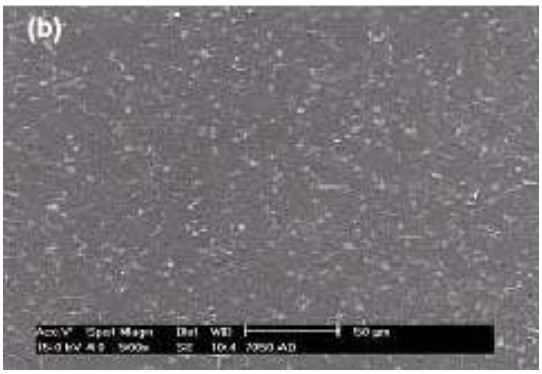

Element	Light Phase wt.%	Dark Phase wt.%
Al	66.09	93.41
Cu	11.93	0.78
Mg	8.15	2.16
Zr	0.20	0.22
Zn	13.48	3.37
Fe	0.15	0.06

Figure 16: SEM photomicrographs of (a) commercial 7050-T7651 plate and (b) as-spray-rolled 7050 (below). Tables summarize EDS composition analysis of phases.

4.3 Scale-Up of Spray-Rolled Strip

The linear atomizer design used to spray roll aluminum strip early in the project has undergone several revisions during the project. Initially, a 1 in. wide linear atomizer was found to routinely spray roll a 3 inch wide strip. Improvements in melt delivery to the atomizer, as well as improved gas/metal mixing in the atomizer, has resulted in the ability to spray roll 4 in. wide strip with a ¾" wide linear atomizer.

The ability to scale strip width by 2X by producing 8" wide strip was demonstrated in two ways. In one of these, for a given roll gap, the deposition rate was doubled while the roll speed was maintained constant. This resulted in significant lateral flow of the semisolid material as it progressed toward the roll gap. Tensile analysis of 3003 strip produced in this way indicated that strip properties at the edge of strips were similar to those along the centerline.

2X scalability was also demonstrated by placing two atomizers side-by-side in such a way that the edges of the spray jets overlap. This approach has proven to be the most reliable method for generating wide strip in alloys with broad freezing ranges.

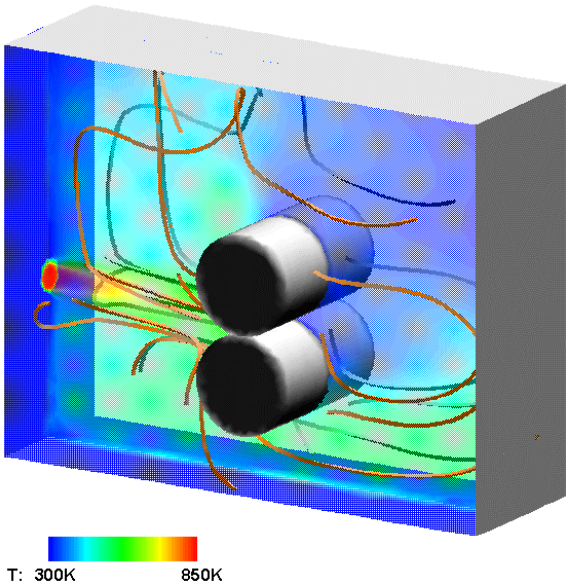

Figure 17: Spray-rolling chamber flow field.

4.4 Characterization of the Flow Field in the Spray Chamber

An important concern in spray deposition processes is that of overspray. Two major factors influence the occurrence of overspray: splashing and/or rebound during the deposition phase and flow field topology in that it conditions the ability of the flow to carry overspray droplets. The former is discussed later in this report. The three-dimensional flow field induced by the spray in the spray rolling chamber was characterized by numerical solution of the steady-state Navier-Stokes and energy equations.

$$\nabla \cdot (\rho \mathbf{V}\mathbf{V}) = -\nabla p + \nabla \bar{\bar{\tau}} + \rho \mathbf{F} \tag{1}$$

and

$$\nabla \cdot (\rho \mathbf{V} H) = \nabla \cdot (\mathbf{V} p) + \nabla \cdot (k \nabla T) + \Phi \tag{2}$$

where ρ is the fluid density and k its thermal conductivity, $\mathbf{V}$ the velocity field, p the pressure field, $\bar{\bar{\tau}}$ the stress tensor, $\mathbf{F}$ a body force (such as gravity), H the enthalpy field, T the temperature field, and Φ the viscous dissipation. A CFD code, CFD-ACE (CFDRC, Huntsville, AL), was used for that purpose.

In the example of the case shown in Figure 17 (gas jet injected at 850 K and 45 m/s, rolls at 300 K), the pathline pattern clearly shows how the asymmetric position of the rolls in the model chamber induces a corresponding asymmetry in the flow field. As reported below, this asymmetry has a direct effect on the spray behavior. In addition to providing a clear picture of the flow patterns in the chamber, these simulations allowed the identification of the effect of changes in chamber configuration (such as the nozzle-to-roll distance) on this environment [12].

It became clear, early in the process development, that some of the questions that were arising regarding the spray topology and overall behavior (such as: *"What is the thermal energy content*

of the spray at impact?") should be answered theoretically/numerically so that various development options could be considered. A polydispersed spray model, outlined below, which couples a three-dimensional flow field simulation to particle tracking and heat transfer models was built for that purpose. The coupling is done in a one-way manner to preserve computational efficiency. Heat transfer and solidification is modeled with a multi-stage lumped parameter approach, which includes the influence of rapid solidification.
The flow of the carrier gas is solved numerically as indicated in the previous section. The continuous phase conservation equations are solved without coupling to the dispersed phase momentum, heat and mass transfer. This procedure eliminates the costly iterations between continuous and dispersed phase calculations, and allows the simulation results to be calculated once and used as an interpolation library for repeated dispersed phase calculations. However, one-way coupling is only valid for dilute sprays and suffers from some inaccuracy near the atomization region.

To model the spray as a whole, it is not practical to calculate the trajectories of every droplet within the spray. A more pragmatic approach is to discretize the spray into computational particles, for which the trajectories and thermal histories are calculated. Those trajectories are integrated downstream to reconstruct the spray as a whole. To this end, the spray is modeled with distributions for the initial droplet size (D)

$$g_D(D) = \frac{1}{\sqrt{2\pi}\,\ln\sigma_D}\exp\left[-\frac{\left(\ln D - \ln D_m\right)^2}{2\ln\sigma_D^2}\right] \tag{3}$$

and speed (c),

$$g_c(c) = \frac{1}{\sqrt{2\pi}\,\sigma_c}\exp\left[-\frac{\left(c-\mu_c\right)^2}{2\,\sigma^2}\right] \tag{4}$$

Computational particles are sampled randomly from these distributions and their trajectories and thermal histories are calculated as described below.

The calculation of the conditions of the continuous phase at the location of a given particle requires knowledge of the particle location, with respect to the continuous phase grid. For this purpose, the continuous phase simulation results are maintained as an interpolation library composed of tetrahedral cells. To calculate the interpolated values, the cell containing the particle must first be located. In order to minimize computational expense when locating the resident cell, a list of neighbors is maintained for each cell; a neighbor is a cell that shares a common face with the cell considered. With the neighbor list in place, the procedure for locating the cell containing the particle is as follows:

- Check if the particle is still in the same cell that contained that particle during the last time step.
- If the particle is not located in that same cell, determine if the particle is in any of the immediate neighboring cells.
- If the particle is not located in any of the immediate neighboring cells, search through the entire library until the cell containing the droplet is found.

Searches though the entire library are costly, but rare with appropriately small time steps. Once the cell containing the particle has been located, the continuous phase values may be interpolated from the cell vertexes to the particle location. This is accomplished using weighting or shape functions.

It is necessary to have knowledge of the droplet gas relative velocity, and the particle location for evaluation of the continuous phase properties and to determine the influence of the continuous phase on particle solidification and heat transfer. It is also necessary to know particle velocities and positions for reintegration of the spray down stream from injection. To these ends, trajectories for computational particles are calculated using a simplified version of the particle equation of motion.

$$\frac{d\mathbf{V}_d}{dt} = \mathbf{g}\left(1 - \frac{\rho_g}{\rho_d}\right) + \frac{3C_D}{4D}\frac{\rho_g}{\rho_d}\left|V_g - V_d\right|\left(\mathbf{V}_g - \mathbf{V}_d\right) \tag{5}$$

where subscript g refers to the carrier gas and subscript d to the droplet. C_D is the droplet drag coefficient. Droplet solidification is modeled with as multistage solidification process. As a droplet cools and solidifies, the time rate of change of the droplet total enthalpy is balanced by the rate that energy is transferred to the droplet by convection and radiation.

$$\frac{dH}{dt} = \dot{Q}_{\text{conv}} + \dot{Q}_{\text{rad}} \tag{6}$$

The total enthalpy of the droplet is the sum of the enthalpy in the liquid and the enthalpy in the solid.

$$H = m(1 - f_s)\left[C_{p,\ell}\left(T - T_L\right) + \Delta h_f\right] + mf_s C_{p,s}\left(T - T_L\right) + mh_0 \tag{7}$$

m is the droplet mass, f_s its solid fraction, Δh_f the latent heat of fusion, T_L the liquidus temperature, and $C_{p,\ell}$ and $C_{p,s}$ the liquid and solid specific heats. During each stage of the solidification process, the rate of change of the total enthalpy is expressed differently according to the relevant processes and phases present.

During the liquid cooling stage of the solidification process, there is no solid present and no phase change is occurring. Once the nucleation temperature has been reached, rapid solidification occurs and the rate of release of latent heat overwhelms the rate of heat extracted by convection and radiation at the droplet surface. During this stage of solidification the change in total enthalpy is neglected and the post-recalescence solid fraction is calculated by assuming that the post-recalescence droplet temperature returns to the liquidus temperature. In the case where the droplet has become hypercooled, the total available latent heat is not sufficient to bring the droplet temperature back up to the liquidus temperature. When this occurs the droplet is assumed to solidify completely. After recalescence, if the droplet did not experience hypercooling, the droplet undergoes a segregated solidification stage. During segregated solidification, both liquid and solid phases are present and heat extraction at the droplet surface is relevant again. During segregated solidification it is assumed that there is infinite rate diffusion of the solute in the liquid, and diffusion in the solid is neglected. Once the droplet becomes completely solidified, either during the eutectic solidification stage or during recalescence for

hypercooled droplets, the solid cooling stage begins. During the solid cooling stage, there is no liquid present in the droplet and no phase change occurs.

The magnitude of the heating rates experienced by the droplets at recalescence are extremely challenging for the lump parameter analysis employed here. This issue was investigated in the case of pure aluminum droplets by implementing a spatially-resolved solution of the energy equation in each droplet. The results obtained showed that using a lump parameter approach during the recalescence phase produced non-negligible errors on the predicted droplet surface temperature. This is particularly relevant when surface chemistry (e.g. oxidation) is considered. Oxidation is typically avoided in spray processes. However, previous studies [13] have shown that the dispersoids resulting from the shattering of the oxide film that forms in-flight on droplets during spray deposition could promote grain refinement. Consequently, an oxidation model developed at UCI was implemented here to allow a limited investigation of the effect that oxidation my have in the spray rolling process. Some of those results are briefly discussed in the sub-section related to process-scale behavior below.

Once the particle trajectories have been calculated, it is necessary to relate that Lagrangian data to Eulerian data for the spray as a whole. This is accomplished by using the fact that in the Eulerian reference frame the trajectories do not represent a single particle, but rather, a stream of particles with a constant flow rate. The particle flow rate may be related to the linear density along the trajectory and used to calculate Eulerian spray properties by summing over all the particle classes in a control volume.

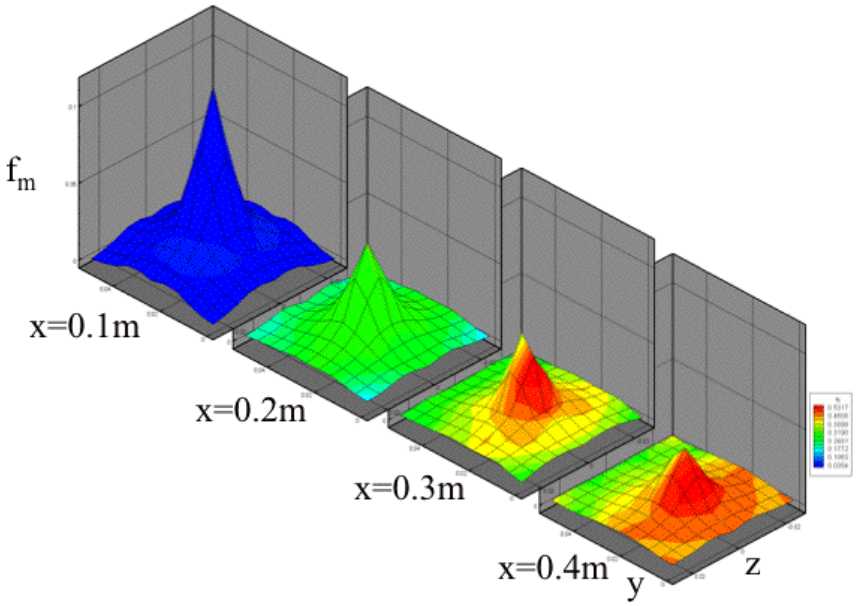

Figure 18: Predicted spray distribution (normalized mass flux) at various axial locations (pure Al). The color contours represent the solid fraction from 0 (blue) to 1 (red).

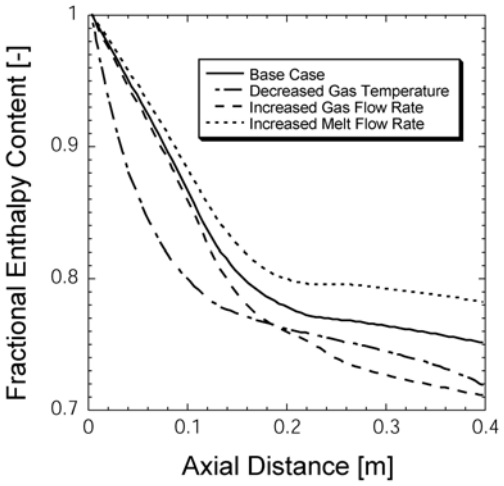

Figure 19: Fractional enthalpy content of the spray.

When used in conjunction with a pre-calculated flowfield such as that discussed above, a comprehensive description of the spray topology and behavior can be obtained. Typical results for the case of pure aluminum are shown in Figure 18. It was consistently found that the solid fraction in the spray at a given axial location is not uniform. Instead, it is higher in the core and decreases moving away from the axis. This is due to the effect that a droplet's size has on its trajectory and history. Larger droplets tend to adopt a more inertial trajectory than smaller ones and, therefore, they can be found in larger numbers away from the spray axis. Indeed, our simulations confirm that the mean diameter is noticeably smaller near the core of the spray than at the periphery. Because smaller droplets have a larger area to volume ratio they undergo larger heat transfer rates and solidify faster.

In the Base Case presented in Figure 19 (gas injected at 450 SLPM and 850 K and liquid metal flow rate of 0.05 kg/s with a superheat of 100 K), about 2/3 of the enthalpy present in the spray at injection is left 40 cm from injection. A limited parametric sensitivity study showed that this enthalpy content at a given axial location can be decreased by decreasing the temperature of the carrier gas or increasing its flow rate (which produces smaller droplets with more efficient heat transfer). Conversely, increasing the melt flow rate produces larger droplets with relatively less efficient heat transfer, which results in a markedly larger enthalpy content at a given axial location [14].

The spray behavior predicted by the polydispersed spray model was compared to experimental data obtained at UCI. The comparison indicated a significant discrepancy between the simulation results and the data. However, it is noted that the only process parameter values available for these experiments were the melt pressure and the gas pressure. This information is insufficient to fully define the flow system and the initial conditions for droplet size and velocity distributions. While it might have been possible to determine initial conditions that produce a better match between the simulation and the available data, the value of such an *a posteriori* run would have been very limited. Validation of the integrated model will require a fully characterized set of experiments [15].

4.5 Droplet Impact, Spreading and Solidification

Two perspectives are relevant in considering the physics of the deposition process: single droplet behavior and collective behavior generated by the impinging spray. In the latter, computational efficiency is necessary so that an adequate number of computational droplets can be considered. On the other hand, considering single droplet behavior using detailed numerical simulation will yield valuable information regarding splashing and will provide a solid base for the validation of coarser impact models but will require significant computational resources.

Whatever the perspective, the configuration of interest for the analytical droplet impact model is a droplet impacting at an angle on a solid substrate (Figure 20). After impact, the droplet spreads and may solidify.

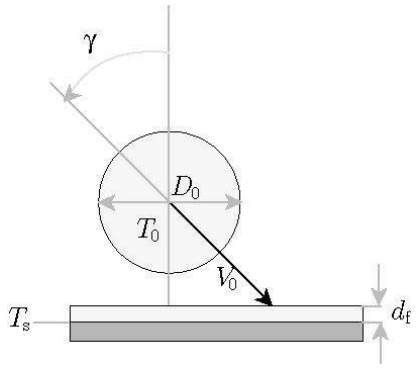

Figure 20: Grid refined around the surface of a droplet.

Integral Description of Droplet Impacts:

An integral approach, based on a mechanical energy balance, is used to model this scenario. A velocity field and a splat shape are prescribed in a manner allowing for a realistic representation of an angled impact. Furthermore, solidification is modeled with or without the influence of thermal contact resistance.

The integral approach used here requires that the problem domain (splat shape) be prescribed. The splat shape is a specified with a uniform thickness and a limaçon is used to specify the perimeter of the splat. The integral method also requires that the velocity field inside the splat be prescribed. Adequate representation of an off-normal droplet impact requires a three-dimensional velocity field; furthermore, the velocity field chosen for the droplet impact problems should satisfy the following constraints: the no-shear condition at the free surface, the no-slip condition at the solid-liquid interface and the incompressible continuity equation.

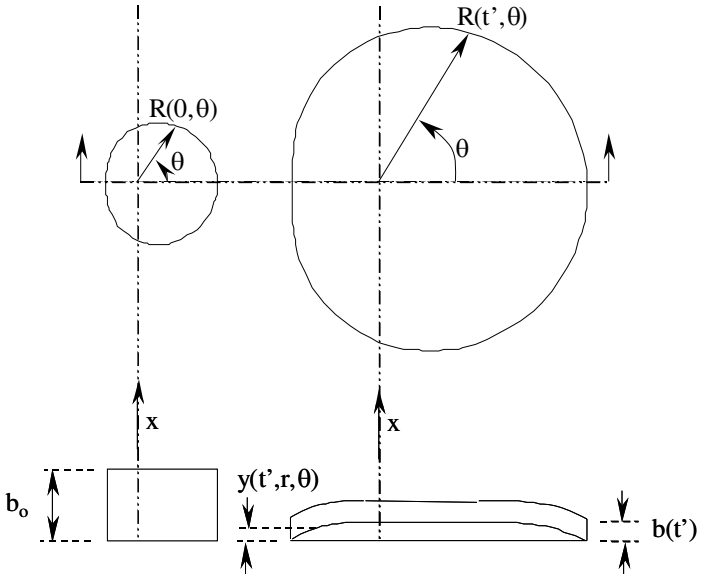

Figure 21: Schematic illustration of splat shape.

With the splat shape and velocity field specified, a mechanical energy balance is used to describe the time evolution of the deforming splat after impact:

$$\frac{dE_k}{dt} + \frac{dE_p}{dt} + \frac{dE_d}{dt} = 0, \tag{8}$$

where E_k is the kinetic energy of the droplet, E_p is the potential energy associated with surface tension, and E_d is the mechanical energy lost through viscous dissipation. The droplet spreading and solidification dynamics is then obtained from the solution of the following non-dimensional integro-differential equation:

$$\frac{d}{dt}\left[\frac{3\varepsilon}{10}\xi^2\phi\left(a_1\xi^2 + \frac{11}{7}\phi^2\right) + \frac{\xi}{\mathrm{We}}\left(\xi + a_2\phi\right)\right] + \frac{\xi^2\dot{\xi}^2}{\phi\mathrm{Re}}\left(a_3 + a_4\frac{\phi^2}{\xi^2}\right) = 0 \tag{9}$$

ξ is the spread factor, ϕ the non-dimensional liquid thickness, Re and We the Reynolds and Weber numbers.[1] In order to evaluate the liquid thickness, the solid fraction must be determined. Solidification is assumed to begin as soon as the droplet contacts the substrate and the location of the solid front can evaluated using the one-dimensional Stefan approximation. However, experiments have shown that a significant thermal contact resistance exists at the substrate splat interface, and heat transfer is likely interface-limited. For solidification with interface-limited heat transfer, and no superheat in the droplet prior to impact, the thickness of the solid layer can be expressed by a linear relationship to time as appose to the square root time dependence found with perfect thermal contact.

[1] Coefficients $a_1 - a_4$ are defined in *Modeling and Numerical Simulation of Droplet Spreading and Solidification after Impact on a Solid Substrate*, by S.B. Johnson, MSc. Thesis, Colorado School of Mines, 2001.

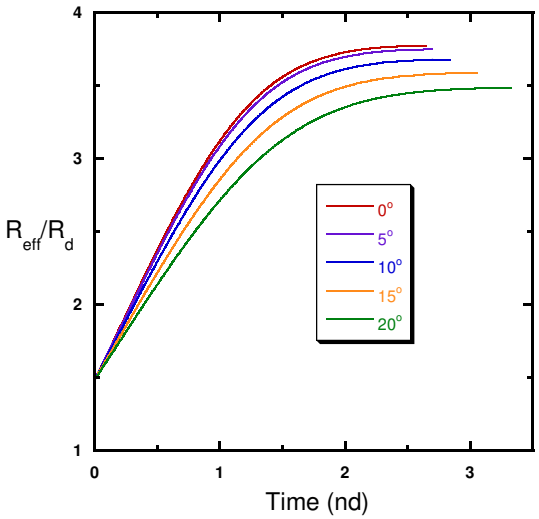

Figure 22: Droplet spreading dynamics.

The efficiency of this integral model allows extensive parametric studies. Results show that increasing the impact angle enhances the viscous dissipation rate, which causes the average spreading rate, the final solid fraction, and the final effective radius (see Figure 22) to decrease. The relative effects of Re, We, and a non-dimensional solidification parameters on that behavior were also thoroughly investigated and documented [16].

While the thermal contact resistance between the spreading splat and the substrate is rarely known, and investigation of its effect on the predicted spreading behavior showed that it plays a determining role (Figure 23).

Comparison of the analytical model to experimental results has indicated that the model tends to over predict the extent to which a droplet will spread (Figure 24). It was identified that the choice of initial conditions was largely responsible for this discrepancy, but problems arose when trying to correct the initial conditions, i.e. the formulation was not consistent with all droplet impacts. Work to reformulate the model using a spherical cap and a cylinder has progressed and shown considerable promises towards resolving the discrepancies between the model and experimental results.

Detailed Description of Droplet Impacts:

As stated previously, numerical simulation of droplet impact is too computationally intensive to be included as part of the integrated process model. However, numerical simulation is still an important part of the overall modeling process. The higher level of accuracy and detail obtain with numerical simulation of droplet impact can be used to validate and make improvements to the analytical model. Two similar interfacial flow solvers have been incorporated into the modeling process for this purpose.

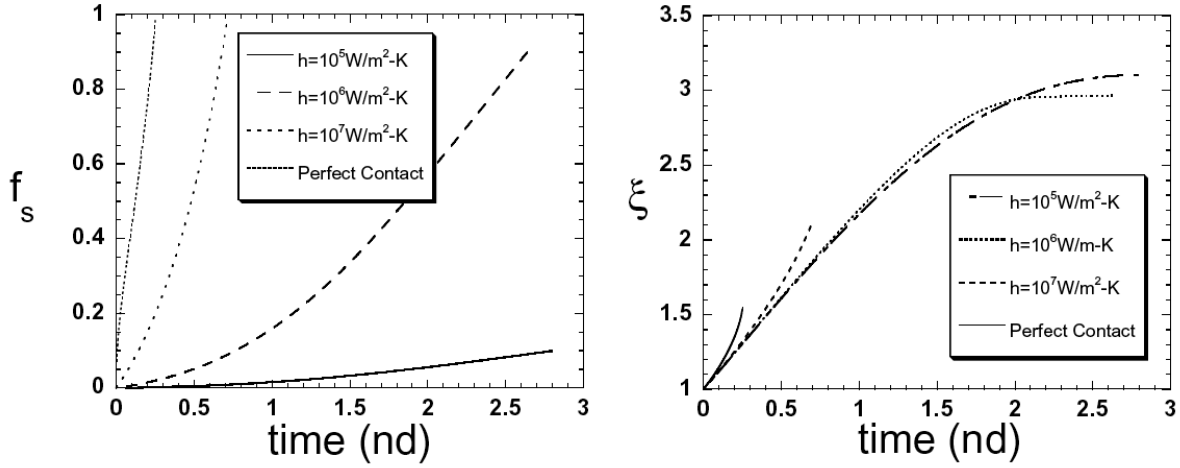

Figure 23: Comparison of the predicted spreading and solidification behavior of an aluminum droplet for various value of the thermal contact resistance

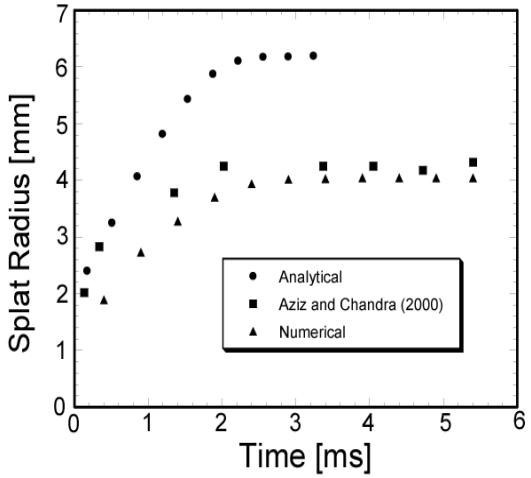

Figure 24: Droplet spreading dynamics.

The first solver is an extension of an existing axisymmetric interfacial flow solver base on the volume-of-fluid (VOF) method, RIPPLE (LANL, Los Alamos, NM). RIPPLE solves the Navier-Stokes equations on a staggered grid using a two-step projection method. Fluid volumes (F) are governed by

$$\frac{\partial F}{\partial t} + \nabla \cdot (F\mathbf{V}) = 0 \tag{10}$$

and tracked using a simple linear interface calculation (SLIC) method, and surface tension is approximated using the continuum surface force (CSF) model.

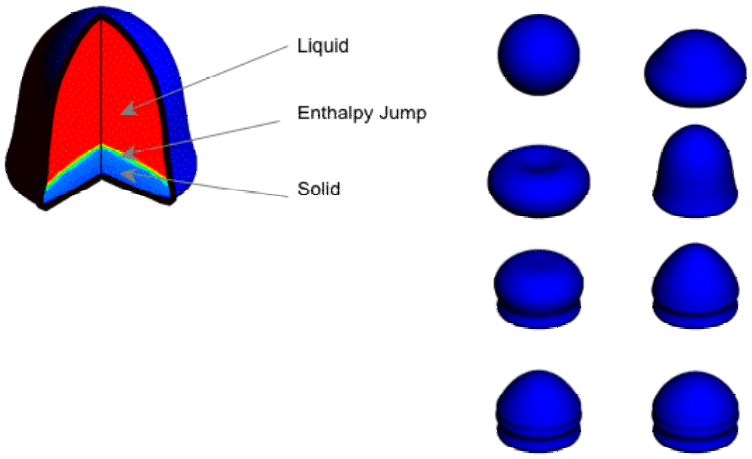

Figure 25: Solder droplet deposition.

This solver was extended to include the solution of the energy conservation equation, and a solidification model to evaluated the influence of solidification on the flow field. This solver is for axisymmetric and two-dimensional flow, and hence, is only suitable for normal droplet impacts (see, for instance, Figure 25), without any three-dimensional phenomena, such as splashing.

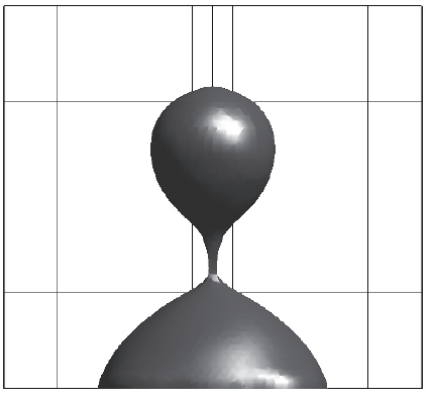

Figure 26: Partial rebound of a droplet recoiling from an impact at Re = 200 and We = 40 with a Bi = 0.05.

To address the three-dimensional aspects of droplet impacts, a three-dimensional interfacial flow solver was developed. This solver uses a colocated finite volume method to solve the Navier-Stokes equation with a two-step projection method, where a Rhie-Chow type correction is made to avoid pressure velocity separation. Fluid volumes are tracked with a more accurate, piece-wise linear interface calculation (PLIC) method. Similar to RIPPLE, surface tension was modeled with the CSF method. However, in this case, a semi-implicit formulation was used to reduce the occurrence of spurious currents associated with inaccuracies in the calculation. Heat transfer and solidification where modeled in the same manner as with the other solver.
The three-dimensional simulations enabled the investigation of three basic impact outcomes as they relate to potential overspray: droplet spreading, rebound (Figure 26) and splashing (Figures 27 and 28) [17]. The droplet spreading study looked at how large of a role viscous and

surface tension effects play in droplet spreading; various impact angles were considered. The droplet rebound study investigated the likelihood that a droplet (or part of it) might detach from the substrate after impact as well as the influence that solidification plays on droplet rebound. The splashing study investigated the influence of increased inertial effects of the formation of instabilities on the edge of a spreading droplet and that of substrate conditions on the formation of a crown.

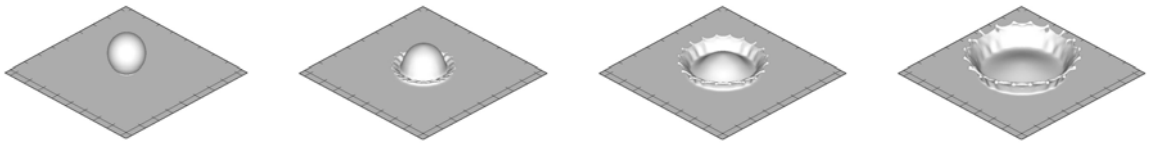

t^*=0 0.65 1.3 2.1

Figure 27: Molten aluminum droplet splashing on a liquid film.

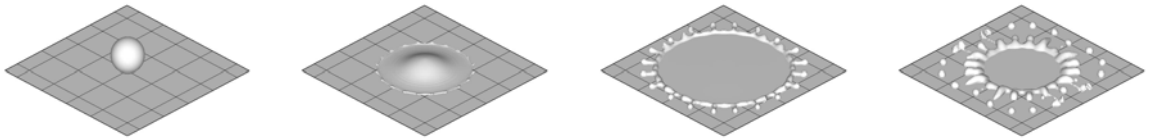

t^*=0 0.65 1.3 2.1

Figure 28: Molten aluminum droplet splashing on a dry substrate.

It was found that viscosity and surface tension significantly influence droplet spreading throughout the range of relevant Reynolds and Weber number. Lower Weber and Reynolds numbers decrease spreading by increasing the rate at which kinetic energy is converted to surface energy and thermal noise. It was also found (confirmed) that higher impact angles decrease spreading of a droplet by displacing the droplet rather than spreading. These results indicate that to model a droplet impacts effectively for spray rolling viscosity, surface tension and the impact angle must all be accounted for. The maximum extent to which droplets spread was relatively small, which is likely contribute significantly to the formation of interstitial porosity.
The investigation of droplet rebound indicated that for the Reynolds and Weber numbers of interest for spray rolling, droplets will rebound if no solidification occurs. The high tendency to rebound was shown to largely be a factor of the high contact angle imposed in the current studies, but the contact angle is necessarily high to keep the strip from sticking to the rolls during spray rolling. Therefore, a high rate of heat extraction is necessary to initiate solidification before droplets recoil. If the heat extraction rate is too low, droplet may partially or completely detach from the substrate, and contribute significantly to overspray.

In spray rolling, only a small portion of droplets have enough inertia to produce splashing. It is therefore unlikely that splashing will have as significant an effect on the formation of porosity as the low degree of spreading that is attained by most droplets. However, splashing may contribute significantly to overspray, depending on the relative importance of droplet rebound.

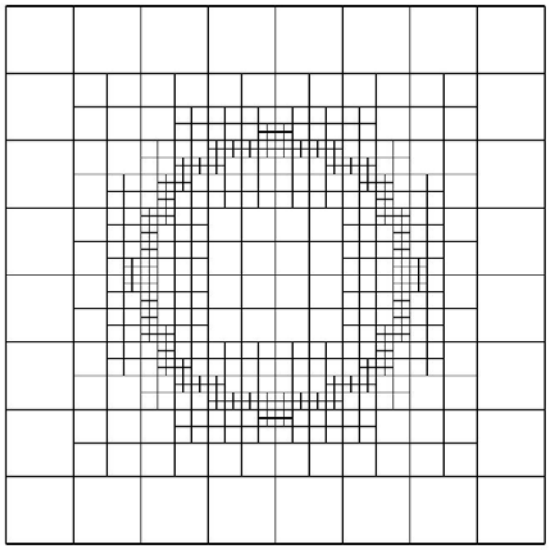

Figure 29: Grid refined around the surface of a droplet.

As shown above, droplet impact involve a wide range of length scales, where the secondary droplets produced during splashing can be an order of magnitude smaller than the initial droplet. This makes it difficult to adequately resolve the small-scale features, while maintaining reasonable computational times. Typical droplet impact simulation for cases with CPR = 15 take roughly 6 hr to compute on a 3 Mhz Pentium Xeon processor, while cases computed using CPR = 20 take roughly 12 hr.

Adaptive mesh refinement was identified as an approach for mitigating this problem. Steps have been taken to implement adaptive mesh refinement in the three-dimensional interfacial flow solver, and to parallelize the solver (Figure 29). This is being accomplished using PARAMESH, a numerical library for parallel adaptive mesh refinement developed at the NASA Goddard Space Flight Center under the HPCC and ESTO/CT projects [18].

4.6 Process-Scale Behavior

The efforts described so far provide detailed and focused insight regarding specific sub-processes (e.g. spray transport and solidification or droplet impact and spreading). In order to address overarching issues related to the development of the spray-rolling process, such as overspray and process scale-up, the ability to calculate spray history throughout the process, from atomizer to roll bite, is required.

Given the wide range of length scales inherent to spray rolling sub-process models (most of which are described above) adapted to the relevant scales (droplet, spray, chamber) were integrated to form a total process model (Figure 30). Spray rolling can be broken down into atomization, in-flight quenching, deposition, and rolling.

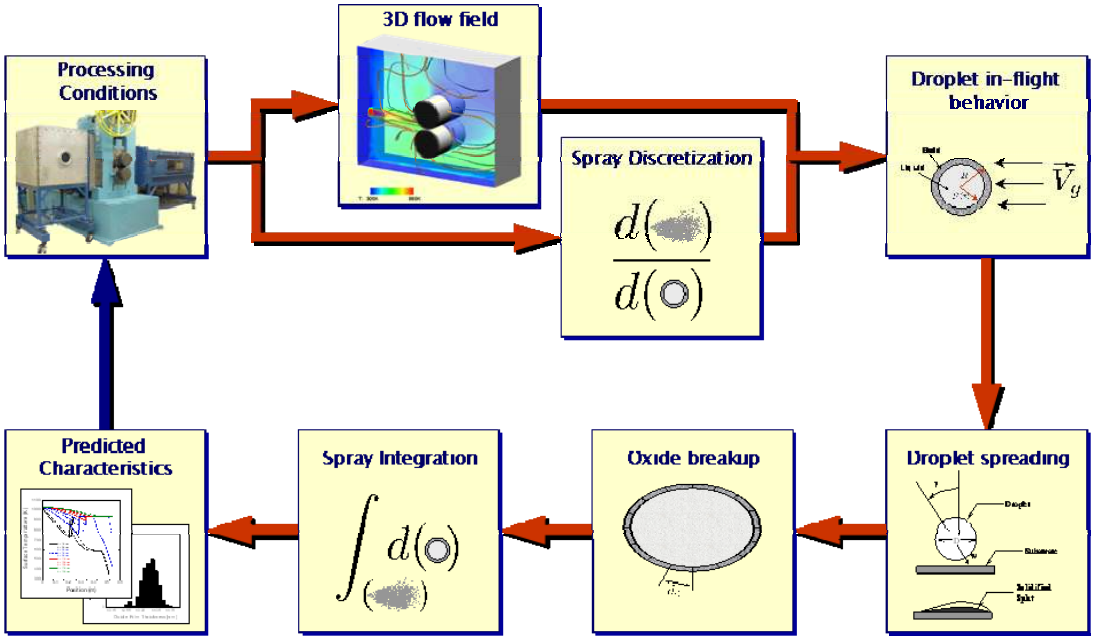

Figure 30: Integrated process model synopsis.

The procedure for the integrated process model is therefore as follows:

- Using the spray-rolling process parameters and the Lubanska correlation determine the distributions for droplet initial conditions (velocity and size) and the continuous phase flow field.
- Discretize the initial droplet distributions using a Monte-Carlo approach to obtain a number of computational or representative droplets.
- Calculate the trajectories and thermal histories of each of the computational droplets, using the initial conditions from the discretization.
- Calculate the deformation of the droplet during impingement on the mill rolls, calculating the conditions at impact from the thermal histories and trajectories calculated above.
- Re-integrate the spray conditions from the computational droplet to determine spray properties.
- Compare results to the spray rolling process to determine points of improvement for the model.

The major building blocks (sub-process models) needed to put together the integrated process model have been described above. An example of the type of insight that the integrated process model is provided in Figure 31. The case considered here is that defined above with 10% oxygen in the carrier gas. Figure 31 shows the predicted oxide film thickness distribution in the spray right before impact, the spread factor distribution after impact and the resulting dispersoid diameter distribution after oxide film breakup (calculated using a model developed at UCD) [19].

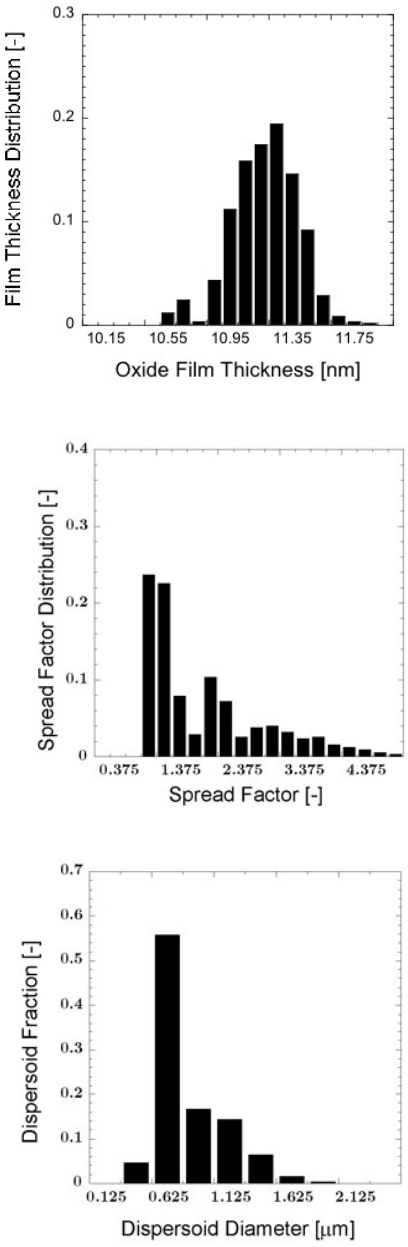

Figure 31: Predicted collective behavior in a reactive flow case.

The oxide film thickness before impact is basically uniform (at about 11 nm). This is expected given the self-inhibiting nature of the oxidation reaction. Smaller droplets have a larger solid fraction at impact and, therefore, spread relatively less than larger droplets, which explains the similarities between the log-normal droplet size distribution in the spray and the shape of the spread factor distribution (the pseudo-multimode character is an artifact of the discretization method used in this particular case). Finally, since larger droplets spread relatively more smaller ones they produce smaller dispersoids and since they carry more mass the dispersoid diameter distribution exhibits a peak (625 nm) shifted to the lower values.

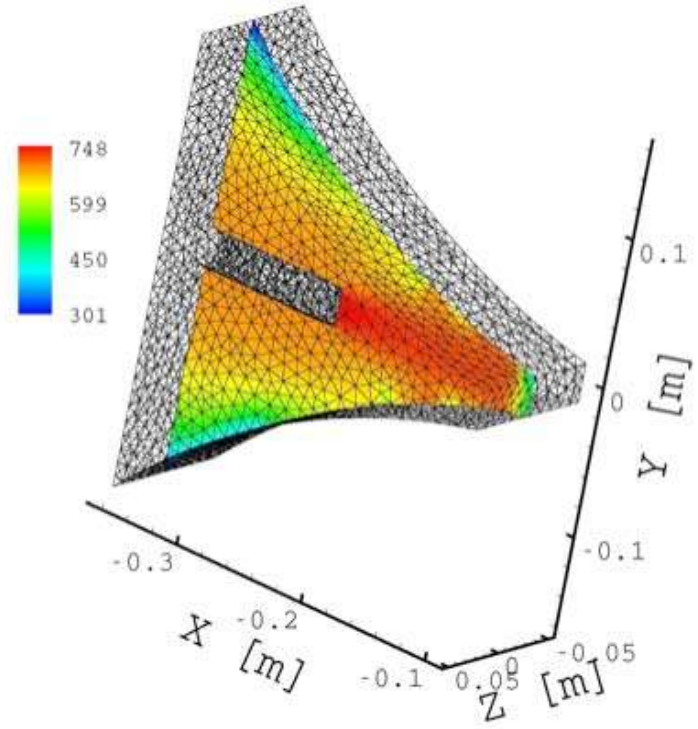

Figure 32: Example of a scale-up study. Predicted thermal field.

Modeling contribution to the preliminary investigation of scale-up issues:
The tools developed to investigate the process development as described above, can be readily utilize to study potential issues associated with process scale-up. While this aspect remained at the preliminary stage, issues such as chamber flow field in a scaled configuration (see Figure 32) and multiple nozzles configurations were explored.

4.7 Modeling Analysis of a Transient to Steady State Transition during Spray Rolling

From the geometrical standpoint, a qualitative geometric analysis was performed and the transient to steady state transition during the spray rolling process was predicted under two cases exist for the evolution of the spray-rolled geometry: 1) $d > D/2$ and 2) $d \le D/2$, where d is the distance between the linear atomizer and the roll-axis plane defined as the plane determined by the two axes of the rolls and D is the roll diameter, as shown in Figures 33 (a) and (b). The analytical results indicate that, when the deposited materials at the specific points on one roll surface overlap their counterparts on the other roll surface, spray rolling transits from the transient state to the steady state. The specific points are the limiting deposition positions of the atomized droplets on the roll surface initially. For the case of $d > D/2$, the limiting deposition positions are points P_1 and P_2 corresponding to the two outer-side tangent lines from the nozzle position N to the two rolls, N P_1 and N P_2 (Figure 33 (a)). For the case of $d \le D/2$, the limiting deposition positions are points L_1 and L_2 which are the intersection points between the roll surface and the straight line normal to the spray axis.

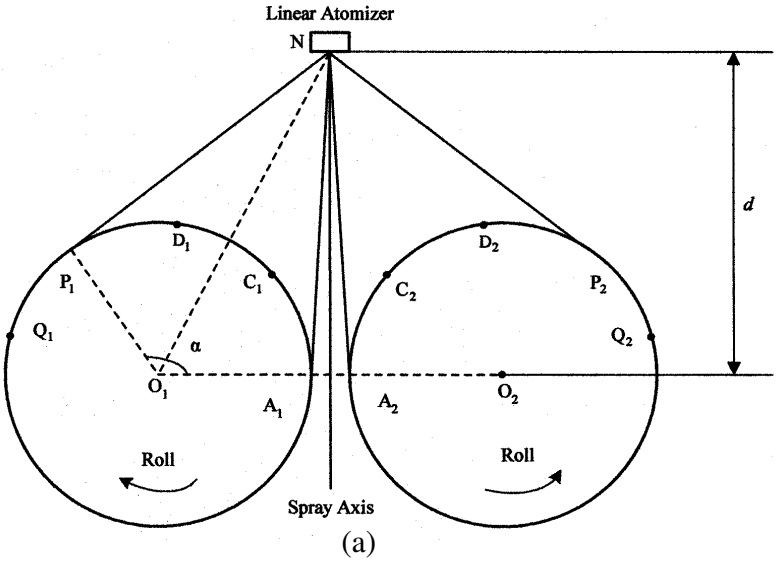

(a)

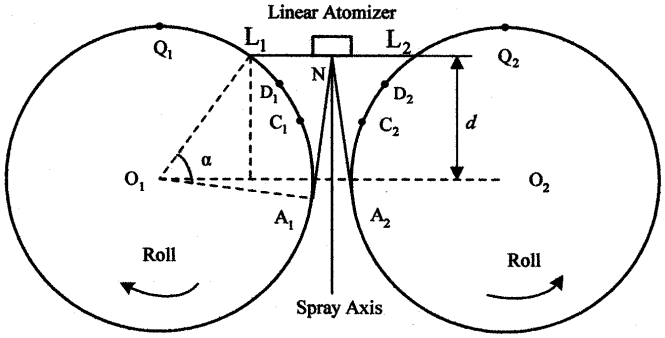

(b)

Figure 33: Geometrical configurations normal to the direction of the roll axes at the initial instant of the spray-rolling process: (a) $d>D/2$, and (b) $d\leq D/2$.

4.8 Model Development and Simulation Analysis of the Maximum and Minimum Spray Deposition Rates during Spray Rolling Process

An analytical model was developed to predict the maximum and minimum spray deposition rates during spray rolling process. In this model, the maximum spray deposition rate is determined by two factors: 1) From the drag-in perspective, the maximum spray deposition rate must be selected such that the rolling angle does not exceed the drag-in angle, $\theta_{drag}=\tan^{-1}\mu$, where is the friction coefficient between the roll and the rolled materials. 2) The maximum spray deposition rate must be selected to ensure a sufficient distance between the nozzle and the deposited surface to obtain a high materials deposition yield. The selection of the minimum spray deposition rate is constrained by the following three criteria: First, the minimum spray deposition rate must be selected to insure the formation of a strip product (Figure 34). Second, the minimum spray deposition rate must be selected to provide a thickness reduction ratio that results in the complete removal of porosity in the deposited material. Third, prior droplet boundaries must also be

removed under the thickness reduction ratio determined by the minimum spray deposition rate so that metallurgical bonding occurs between prior droplets.

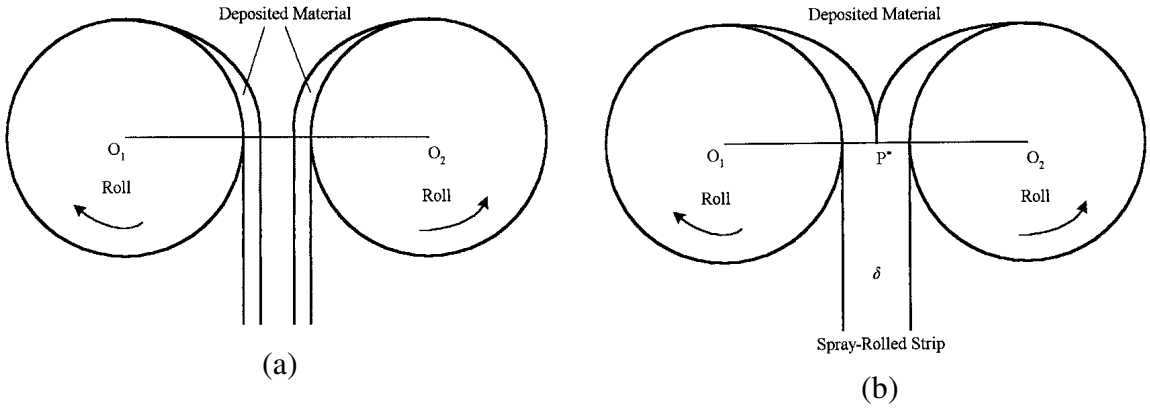

Figure 34: The critical condition for the formation of a spray-rolled strip: (a) no spray-rolled strip formation at low spray deposition rate, and (b) spray-rolling a strip under the critical spray deposition rate.

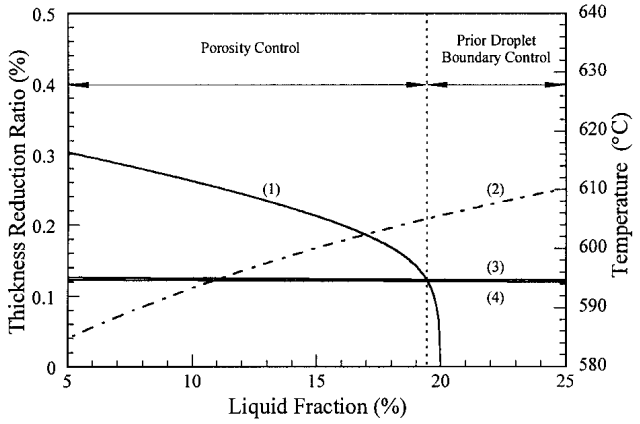

(1): the calculated minimum thickness reduction ratio required to remove porosity.
(2): the temperature of deposited 5083 Al at the deposit/roll interface.
(3): the calculated minimum thickness reduction ratio required to remove prior droplet boundaries at a temperature 40 °C lower than the initial temperature at the deposit/roll interface.
(4): the calculated minimum thickness reduction ratio required to remove prior droplet boundaries under the initial temperature at the deposit/roll interface.

Figure 35: The calculated minimum thickness reduction ratios required to remove porosity and prior droplet boundaries under different initial liquid fractions at the deposit/roll interface.

Based on the above model, the minimum and maximum spray deposition rates have been analyzed. The key factor that may control the minimum spray deposition rate is either the removal of porosity or the removal of prior droplet boundaries. With an increase in initial liquid fraction at the deposit/roll interfaces, the mechanism changes from the former to the latter, as shown in Figure 35. The mechanism that controls the maximum spray deposition rate is related to either the drag-in angle or the distance between the nozzle and deposited material's surface.

With an increase in roll diameter or a decrease in distance between the nozzle and the roll-axis plane, the controlling mechanism is changed from the former to the latter, as shown in Figures 36 and 37. Third, both the calculated maximum and minimum spray deposition rates markedly increase with an increase in roll diameter and roll rotational frequency, as shown in Figures 38 and 39. The above results of theoretical analysis suggest that spray rolling can be optimized to manufacture strips with a high production rate by increasing roll rotational frequency.

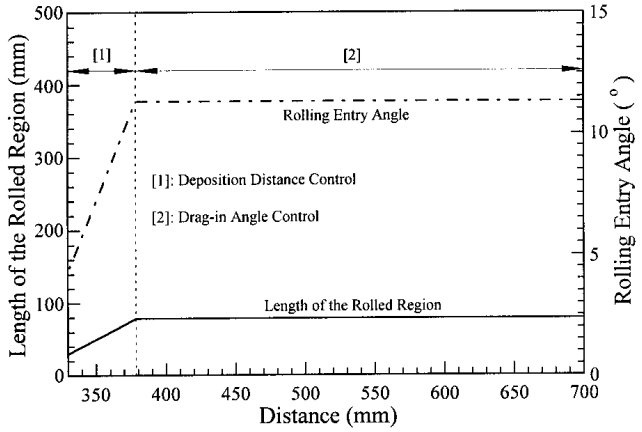

Figure 36: The calculated maximum rolling entry angle and the calculated length of the rolled region as a function of the distance between the nozzle and the roll-axis plane.

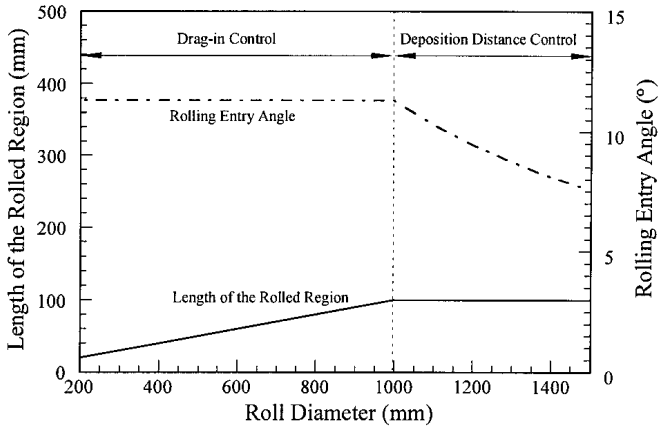

Figure 37: The calculated maximum rolling entry angle and the calculated length of the rolled region as a function of roll diameter.

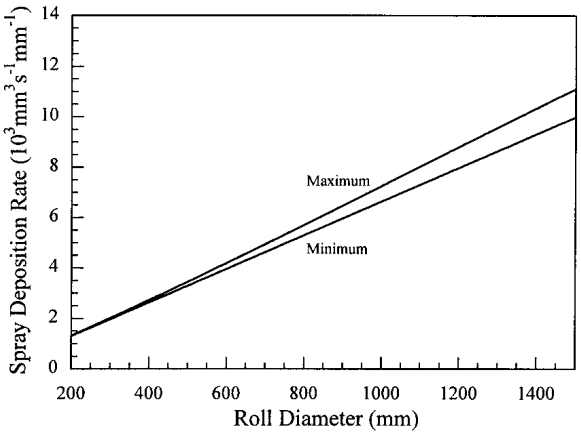

Figure 38: The calculated minimum and maximum spray deposition rates at different roll diameters.

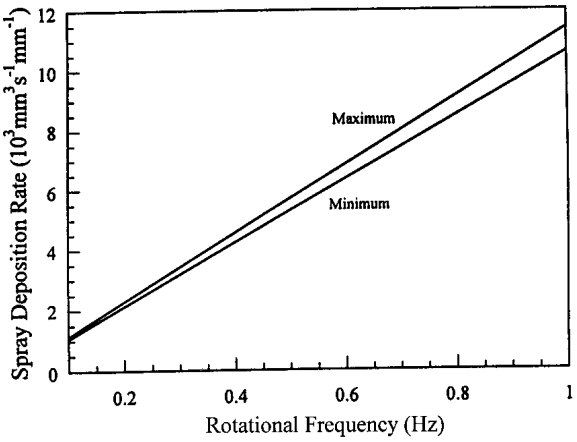

Figure 39: The calculated minimum and maximum spray deposition rates at different roll rotational frequencies.

4.9 Numerical Analysis of Thermal Behavior and Temperature during Spray Rolling

Temperature is a critical factor for: i) the control and optimization of microstructure, mechanical properties, as well as quality of spray rolling, and ii) in-depth understanding of spray rolling process. However, under a regular spray rolling condition, there is a period of less than 1 second from the deposition of material on the rolls to the completion of rolling while the temperature change is significant. It is difficult to perform an in-situ temperature measurement. Thus, it is required to develop a numerical model to calculate the temperature during spray rolling process.

Since width and length of the deposited material or the spray-rolled strip is much larger than thickness, heat transfer during spray rolling can be assumed to be one-dimensional. A one-dimensional numerical model has been developed to deal with heat transfer and thereby temperature during spray rolling (including prior to rolling contact and during rolling). On the basis of this numerical model, the following temperature change can be predicted: i) prior to

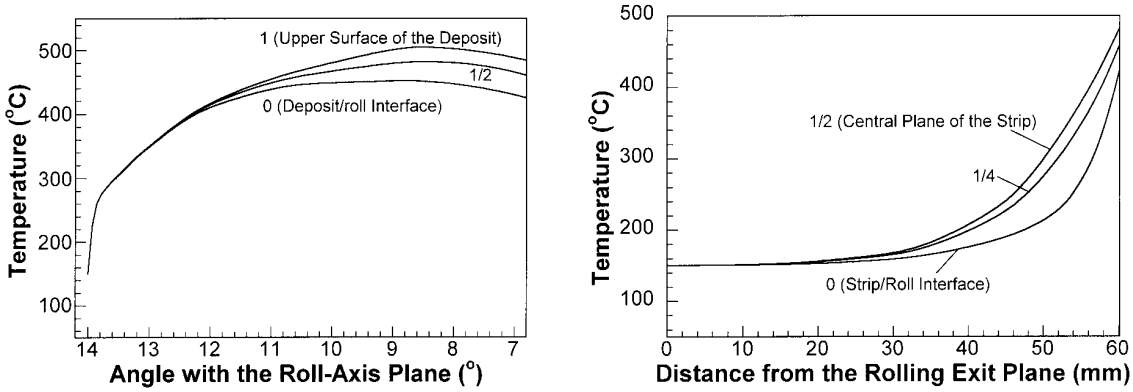

(a) (b)

Figure 40: Temperatures at the different dimensionless thickness during spray rolling of 5083 Al under a low roll rotational frequency of 0.6 rpm: (a) prior to rolling contact, and (b) during rolling.

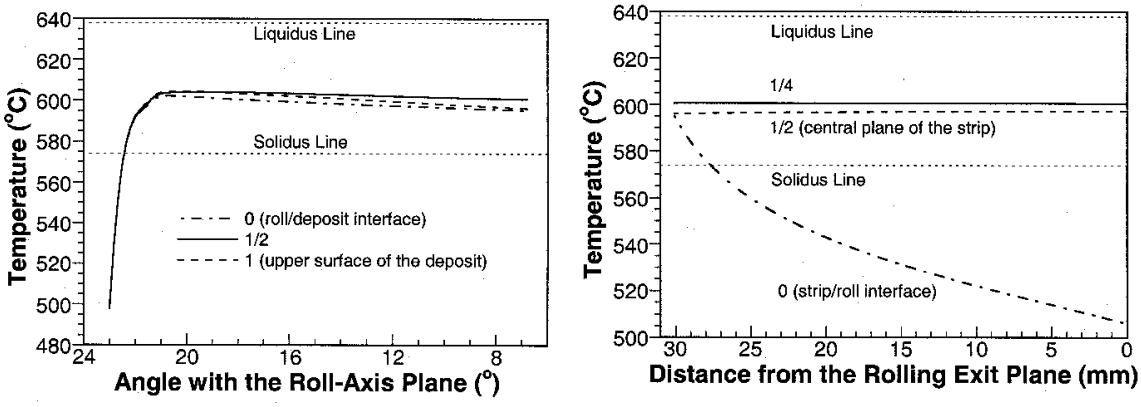

Figure 41: Temperatures at the different dimensionless thickness during spray rolling of 5083 Al under a high roll rotational frequency of 60 rpm: (a) prior to rolling contact, and (b) during rolling.

rolling contact, incoming droplets are first quenched to a relatively low temperature. Then, the temperature of the deposited material increases rather than decrease. When the temperature reaches the maximum value, the temperature slightly decreases until the rolling commences. The temperature rise originates from re-heating of incoming droplets to the previously deposited material. The subsequent slight decrease of temperature can be attributed to the decrease in the deposition rate so that the loss of thermal energy exceeds the heat flux brought by the incoming droplets. On one hand, under a low roll rotational frequency, the maximum temperature prior to rolling contact is lower than the solidus line and the deposited material exhibits a solid state (Figure 40 (a)). On the other hand, under a high roll rotational frequency, the temperature generally increases to above the solidus temperature (Figure 41 (a)). In other words, the deposited material exhibits a mushy state prior to rolling contact. ii) During rolling, under a low roll rotational frequency, the temperature decreases rapidly (Figure 40 (b)). The rapid decrease of temperature is attributed to: a) no heat flux provided, and b) the good contact between the materials and the rolls caused by rolling pressing force, and thereby high interfacial heat transfer coefficient. Under a high roll rotational frequency, the temperature at the interface between the rolls and the deposited material decreases rapidly (Figure 41 (b)). At other thickness, the temperature decreases slightly due to the short time experienced during rolling (high roll rotational frequency), as shown in Figure 41 (b). The calculated results of temperature successfully rationalize the microstructural evolution during spray rolling that has been observed in INL.

4.10 Experimental and Numerical Studies of Reactive Atomization and Deposition (RAD)

RAD, where a reactive gas or gas mixture (e.g., O_2-N_2 in our current project) is used instead of an inert gas, is an approach to optimize microstructure and mechanical properties of a spray-rolled strip. RAD was investigated experimentally and numerically in the following aspects:

Oxidation Behavior during RAD Process

The oxidation behavior of droplets during RAD has been analyzed on the basis of a numerical framework. An equation that represents the growth rate of the oxide phases, together with

models that describe the dynamic and thermal behavior of droplets, is implemented in an effort to elucidate the oxidation behavior of individual droplets. The numerical results reveal that the oxidation rate of a droplet is extremely high and that the oxide phase grows very rapidly initially,

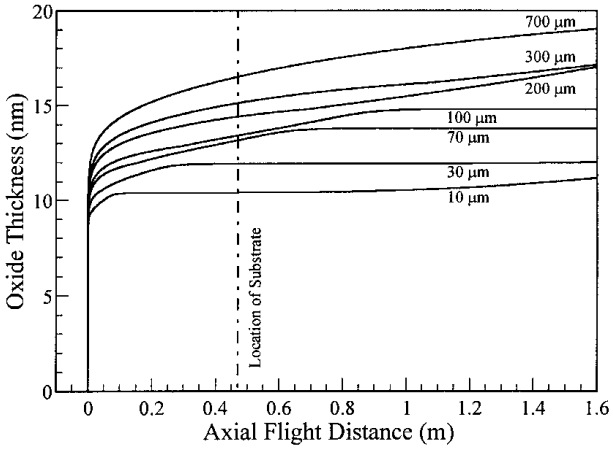

Figure 42: The calculated oxidation histories of individual droplets during RAD.

eventually attaining a steady state of limited oxide growth, as shown in Figure 42. The overall volume fraction of oxide phases in the RAD material increases with increasing atomization pressure, superheat temperature and O_2 concentration, whereas it decreases with increasing melt flow rate, as shown in Figures 43 (a) to (d). The oxygen concentrations in the RAD powders and deposited materials predicted on the basis of numerical analysis are in good agreement with the results from chemical analysis.

Influence of in-situ reactions on grain size during RAD

A fundamental study of the factors that govern grain size of RAD 5083 Al was performed. Microstuctural observation shows that, average grain size in RAD 5083 Al is slightly smaller than that in the material processed via N_2 spray deposition (SDN), as shown in Figure 44. A numerical approach, together with measurements of the temperature histories inside the deposited materials, is implemented to analyze the influence of in-situ reactions during RAD process on the evolution of grain size. The numerical results show that, RAD 5083 Al possesses a slightly higher density of nuclei relative to that present in SDN 5083 Al on a per unit volume of deposited material basis at the beginning of the slow solidification of remaining liquid phase, as shown in Figure 45. Furthermore, the RAD material exhibits a slightly lower coarsening extent during the slow solidification. Grain growth is negligible during the solid-phase cooling. Accordingly, the calculated grain size in RAD 5083 Al is slightly smaller than that in SDN 5083 Al, consistent with the observed results. This research result indicates that grain size refinement is insignificant during RAD.

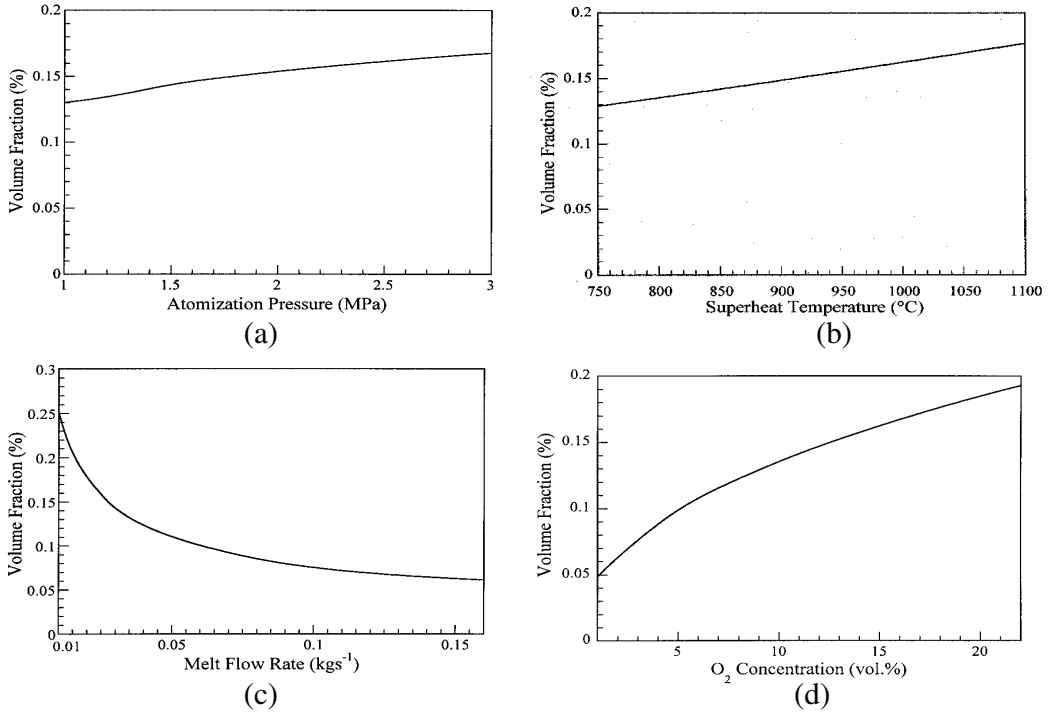

Figure 43: The calculated effect of: (a) atomization pressure, (b) melt superheat temperature, (c) melt flow rate, and (d) O_2 concentration on the overall volume fractions of oxides in the RAD materials.

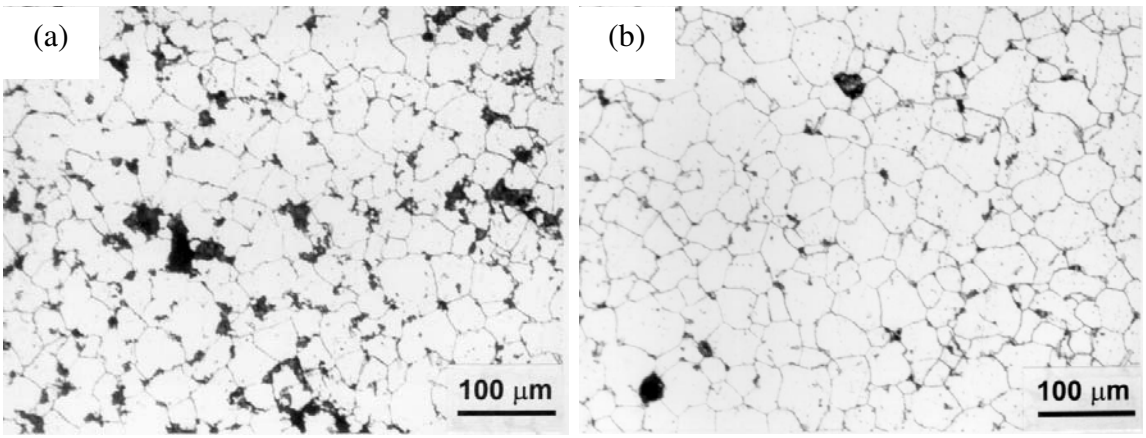

Figure 44: Microstructures of as-deposited 5083 Al under: (a) RAD, and (b) SDN.

Microstructural Characterization of Oxides in RAD Materials

A detailed study of the size, distribution and morphology of oxide partciles in as-sprayed deposited 5083 Al synthesized by RAD was performed. The results indicate that the oxides exhibit a thin-plate morphology and are distributed at prior droplet boundaries, grain boundaries and grain interiors with a dimensional scale on the order of tenths of micrometers up to a few micrometers, as shown in Figures 46 (a) to (d). The mechanisms involved in the formation of the observed oxide distribution are analyzed in detail. The research result indicates that a RAD processing approach, which favors a homogeneous distribution of oxide dispersoids in the worked materials following RAD, is to ensure the average liquid fraction of 20-40% on the deposited material's surface.

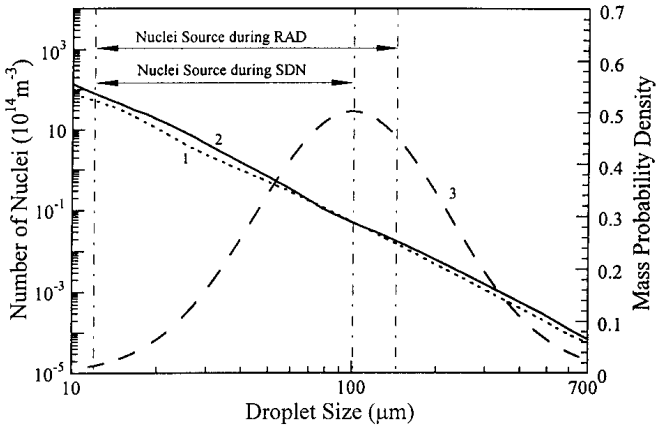

1: number of nuclei in SDN droplets
2: number of nuclei in RAD droplets
3: mass probability density of RAD and SDN droplets

Figure 45: Number of nuclei per unit volume of droplets in the flight stage as a function of droplet size, together with droplet-size distribution.

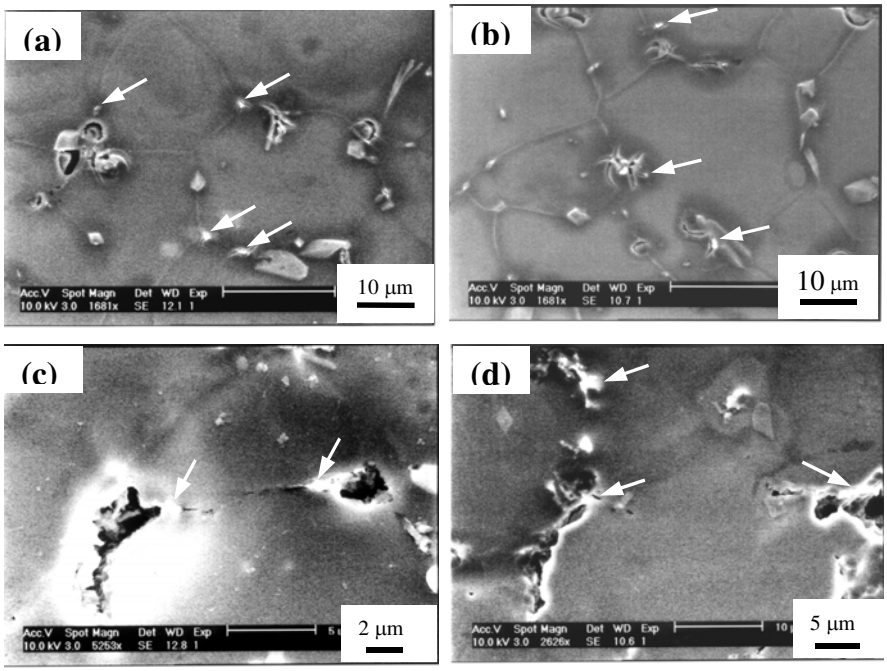

Figure 46: Typical distribution of the oxides in as-deposited RAD 5083 Al: (a) grain boundaries; (b) grain interior; (c) and (d) prior droplet boundaries.

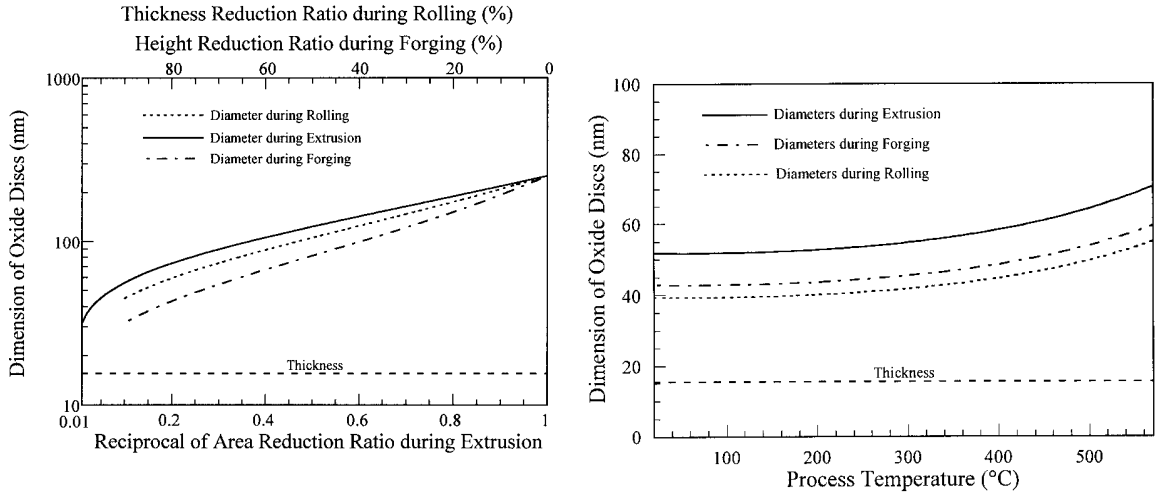

Figure 47: The calculated diameter and thickness of oxide discs as a function of: (a) strain (Left), and (b) process temperature during extrusion, rolling and forging (Right).

Oxide Fragmentation during thermo-mechanical working

An analytical model has been developed to predict the size scale of oxide dispersoids in Al alloys processed by RAD and thermo-mechanical working. The proposed model formulation is primarily based on the assumption that all of the strain energy in the oxides is used to create interfaces between the oxide dispersoids and the matrix. The following predictions are made, based on the above analytical model: i) the diameter and/or thickness of oxide discs (the oxide dispersoids are assumed to have a disc geometry) constantly decrease with increasing strain, as shown in Figure 47 (a). ii) working temperature appears to exert only limited influence on the final diameter and/or thickness of the oxide discs, as shown in Figure 47 (b). The size scale of oxide dispersoids predicted on the basis of the analytical model presented herein is in good agreement with available experimental observations, as shown in Figure 48. This research result indicates that, under a regular spray rolling condition, oxides obtained during RAD (i.e., the spray deposition stage) can be fragmented into fine dispersoids by rolling.

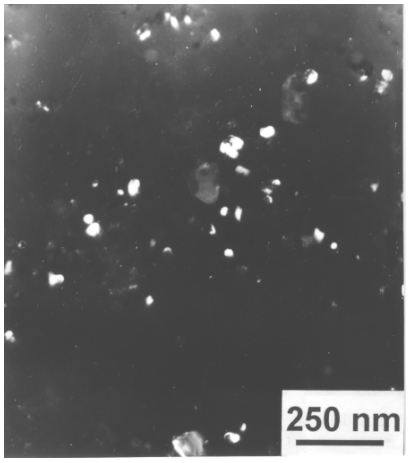

Figure 48: TEM dark field image showing the size of fragmented MgO dispersoids: RAD 5083 Al plus extrusion with the area reduction ratio of 9:1 under 400 °C.

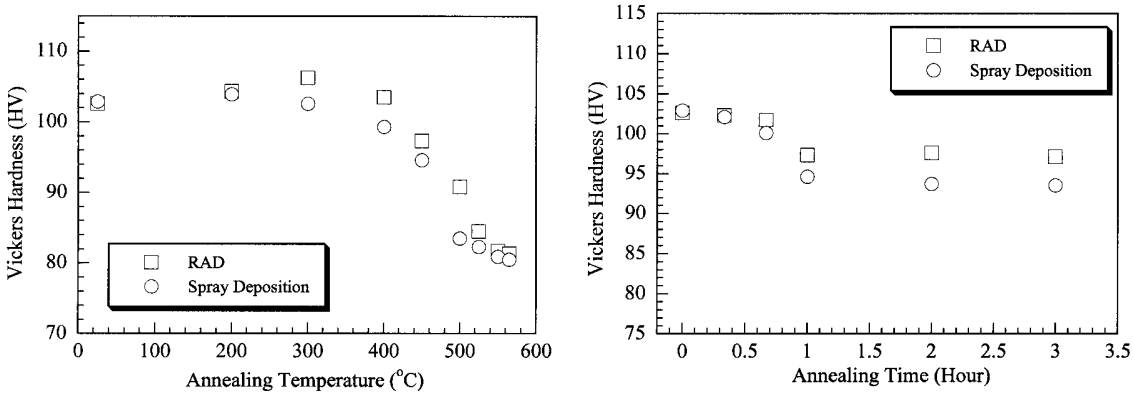

(a) (b)

Figure 49: Vickers hardness of the extruded RAD and SDN 5083 Al as a function of: (a) annealing temperature with an annealing time of 1 hour, and (b) annealing time at an annealing temperature of 450 °C.

Thermal stability of Al alloys processed by RAD and subsequent thermomechanical working

Thermal stability of Al alloys processed by RAD and subsequent thermomechanical working was studied experimentally. Vickers microhardness and tensile properties are measured for the extruded and annealed 5083 Al synthesized by RAD and by N_2 spray deposition (SDN), as shown in Figure 49 and Table 9. The results show a higher thermal stability for RAD 5083 Al compared to SDN 5083 Al, which is primarily attributed to the grain boundary pinning originating from fine MgO dispersoids (Figure 50).

Table 9: Tensile properties of RAD, SDN and commercial 5083 Al.

Source	Process condition	Yield strength (MPa)	Ultimate tensile strength (MPa)	Elongation (%)
RAD	*1	241	381	19
	+2	226	353	17
SDN	1	237	384	19
	2	165	331	27

* 1: extrusion at 400 °C with area reduction ratio 9:1.
+ 2: extrusion at 400 °C with area reduction ratio 9:1 + annealing at 450 °C for 4 hours.

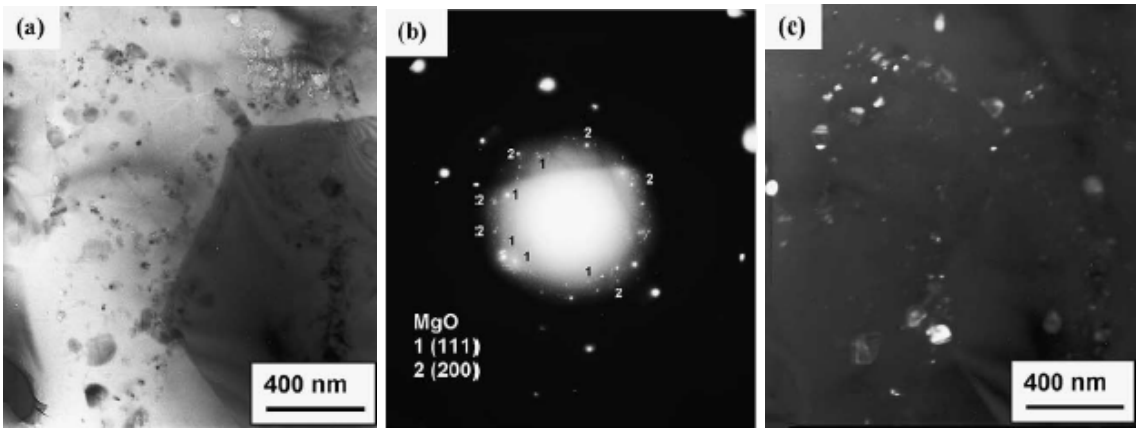

Figure 50: (a) TEM bright field image showing oxide dispersoids, (b) corresponding SAD pattern indicative of MgO, and (c) TEM dark field image from the spots on the second ring.

4.11 Experimental and Numerical Studies of Evolution Mechanisms of Grain Size during Spray Forming

In order to optimize mechanical properties of the spray rolled Al strips, controlling mechanisms in grain size refinement were studied. To fulfill this goal, it is essential to provide an insight into the mechanisms that control grain size. Because the thickness of the spray-rolled strips (1-10 mm) is comparable to the thickness of the initially deposited region during spray forming, the mechanisms of grain size evolution in the initially deposited region during spray forming have been investigated numerically and experimentally, in order to understand the mechanisms of grain size evolution in the spray-rolled strip.

The numerical results show that, in the initially deposited region (1-10 mm), nucleation of incoming droplets occurs during both flight stage and deposition stage. Nucleation events during deposition can significantly refine grain size and generate bimodal grain morphology. As shown in Figure 51 (a), grains smaller than 10 μm take a volume fraction of 40%, indicating grain size refinement. Grain sizes smaller than 3 μm, in the 3-20 μm range and in excess of 20 μm make up the following volume fractions: 34%, 23% and 43%, respectively, indicating a bimodal morphology in good agreement with the SEM observation (Figure 51 (b)). Moreover, the grain size is non-uniform along the thickness. These results are important to modify spray-rolling process: i) to refine grain size using nucleation during deposition and ii) to take measures to minimize the microstructural non-uniformity along thickness.

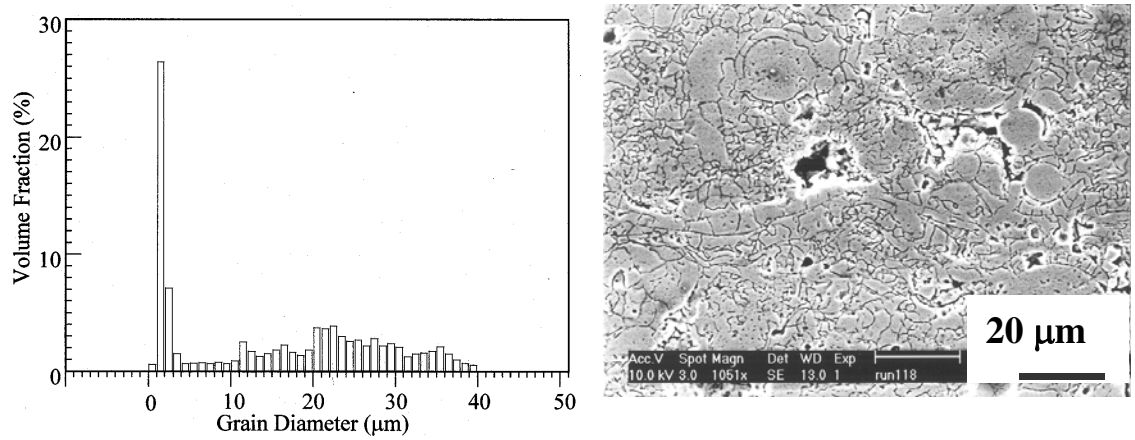

(a) (b)

Figure 51: Grain size and distribution in the spray-deposited material about 2 mm above the substrate: (a) the calculated volume fractions of various sized grains, and (b) corresponding SEM micrograph.

In the region far away from the substrate (e.g., >10 mm in thickness), nucleation of incoming droplets occurs only during flight. As a result, the resultant microstructure exhibits a relatively uniform equiaxed grains. As shown in Figure 52 (a), grain diameters fall in the range of 8.8-53.1 μm. The grains with diameter smaller than 9 μm and larger than 50 μm take low volume fractions, and the grains with diameter between 9 and 50 μm exhibit comparable volume fraction, indicating relatively uniform grain morphology, in good agreement with the OM observation (Figure 52 (b)).

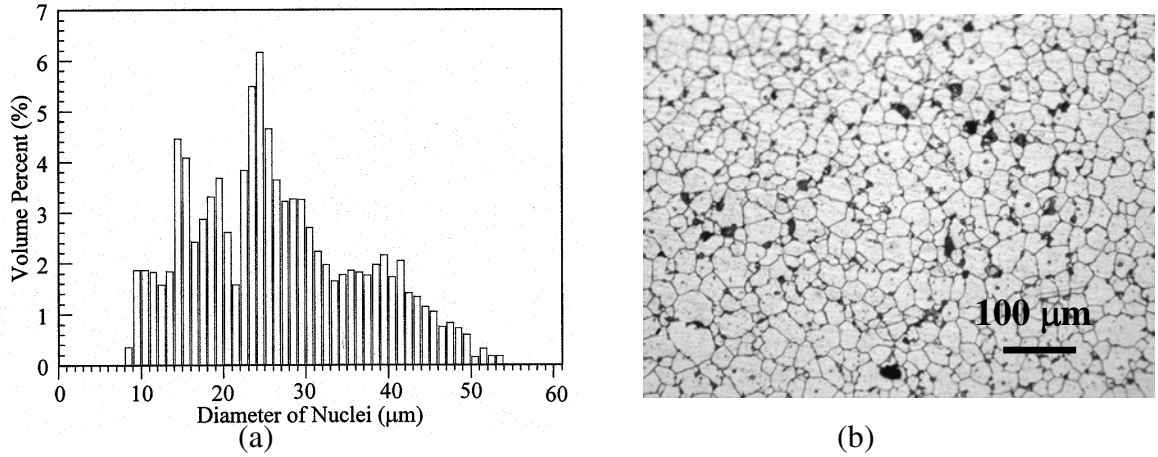

(a) (b)

Figure 52: Grain size and distribution in the spray-deposited material about 2 mm above the substrate: (a) the calculated volume fractions of various sized grains, and (b) corresponding SEM micrograph.

4.12 Microstructural Analysis of Spray Rolled 2124 Al Strip

Microstructural analysis was performed to spray rolled 2124 Al strip under the following processing conditions: atomization pressure 0.14 MPa, melting superheat 100°C, production rate 5.7 m/min and the ratio of the gas to metal flow rate is 0.15 and 0.30.

Figure 53 shows the OM microstructures of as-spray formed 2124 Al under the ratio of the gas to metal flow rate 0.15. The grain size is from 5 to 30 μm. In the plane determined by rolling direction and transverse direction (Figure 53 (a)), the grains are almost equiaxed. In the plane determined by rolling direction and normal direction (Figure 53 (b)), the grains are slightly elongated along rolling direction. The as-spray rolled microstructure was also observed using TEM. In TEM picture as shown in Figure 54, grain size of 1 to 2 μm, different from 5 to 30 μm in OM micrographs (Figure 53). The reason is that TEM analysis can reveals the subgrain structure while OM microstructure cannot reveal subgrains since subgrain boundaries cannot be etched. In order to confirm the existence of subgrains, electron diffraction was made to the four number marked grains in Figure 55 (a). In the diffraction patterns from the four grains (Figure 55 (b)), diffraction spots have a similar arrangement and the difference lies in intensity of corresponding spots. Thus, the four "grains" are actually subgrains from grain "A" (Figure 55 (a)).

Figure 56 shows the OM microstructures of as-spray formed 2124 Al under the ratio of the gas to metal flow rate 0.30. In the plane determined by rolling direction and transverse direction (Figure 56 (a)), grains are elongated along rolling direction. In the plane determined by rolling direction and normal direction (Figure 56 (b)), turbulent flow occurs, leading to grain elongation along various directions.

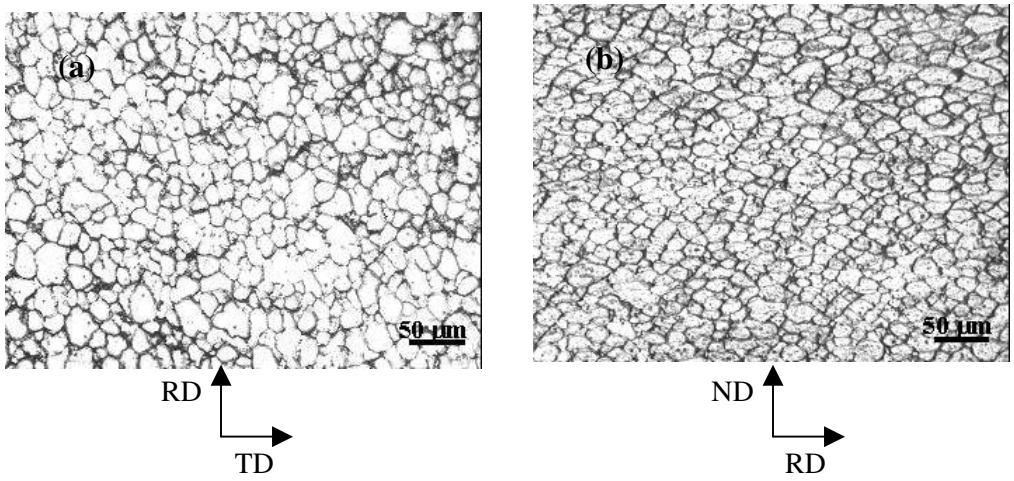

Figure 53: OM micrographs of as-spray rolled 2124 Al under the ratio of the gas to metal flow rate 0.15: (a) in the plane determined by rolling direction (RD) and transverse direction (TD), and (b) in the plane determined by rolling direction (RD) and normal direction (ND).

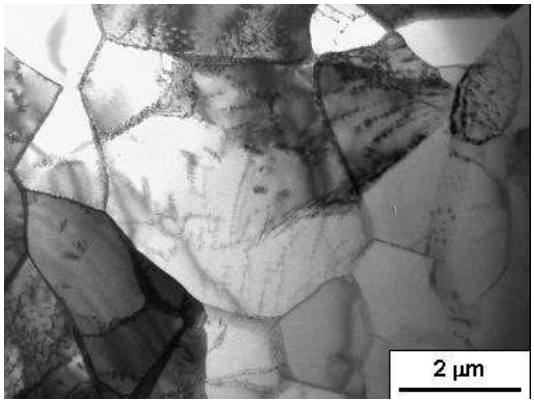

Figure 54: TEM micrographs of as-spray rolled 2124 Al under the ratio of the gas to metal flow rate 0.15 in the plane determined by RD and TD.

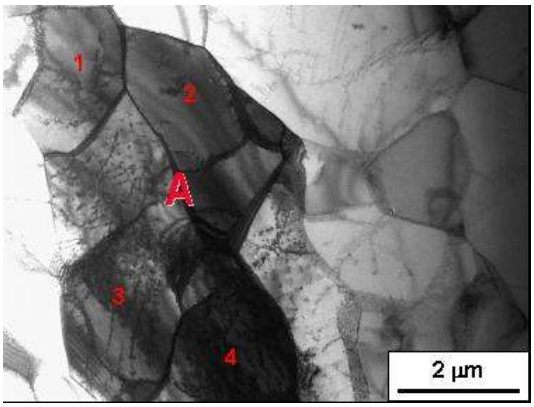

(a)

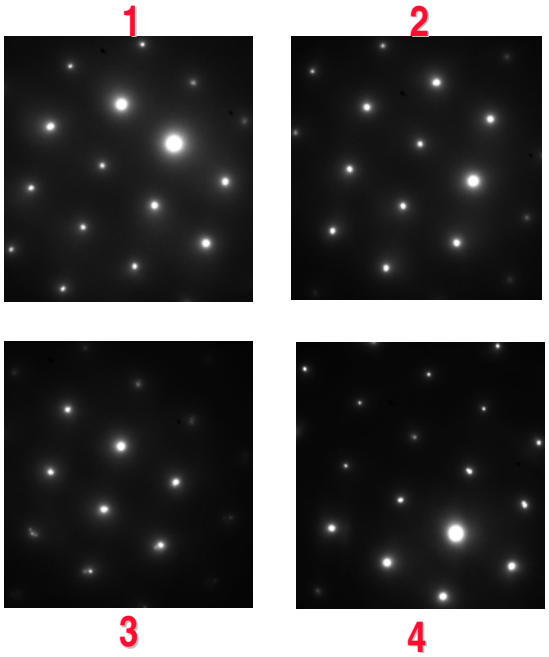

(b)

Figure 55: Confirmation of subgrains: (1) TEM bright field image, and (2) electron diffraction patterns corresponding to the four “grains” in (a).

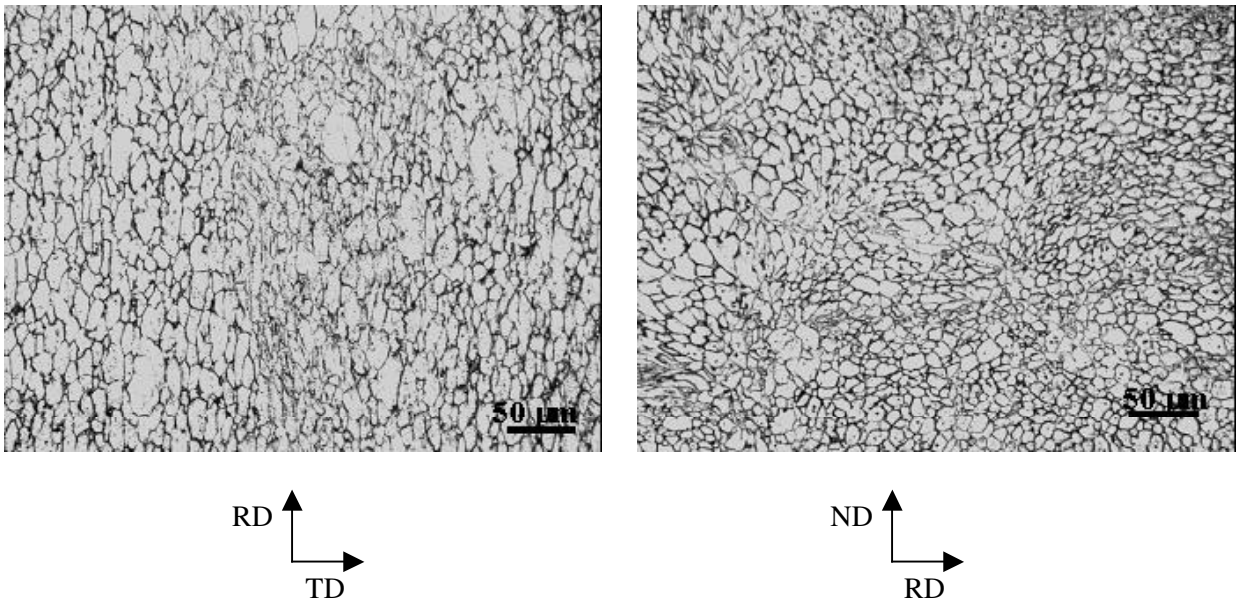

Figure 56: OM micrographs of as-spray rolled 2124 Al under the ratio of the gas to metal flow rate 0.30: (a) in the plane determined by rolling direction (RD) and transverse direction (TD), and (b) in the plane determined by rolling direction (RD) and normal direction (ND).

V. Accomplishments and Technology Transfer

5.1 Journal Publications

Y.J. Lin, J.E. Bobrow, D. White and E.J. Lavernia, "Modeling of Spray Formed Materials: Geometrical Considerations", *Metallurgical and Materials Transactions A,* Vol. 31, No. 11, pp. 2917-2929, 2000.

Y.J. Lin, W. Feng, J. Bobrow and E.J. Lavernia, "Modeling of Spray Formed Plates using X-Y Moving Substrate", *Metallurgical and Materials Transactions A,* Vol. 32, No. 3A, pp. 831-840, 2001.

Kevin M. McHugh, J.-P Delplanque, S.B. Johnson, E.J. Lavernia, Y. Zhou and Y. Lin, “Spray Rolling Aluminum Alloy Strip”, *Materials Science and Engineering A*, Vol. 383, No. 1, pp. 96-106, 2004.

Yaojun Lin, Kevin M. McHugh, Yizhang Zhou and Enrique J. Lavernia, “On the Selection of Spray Deposition Rate during Spray Rolling Process”, *Metallurgical and Materials Transactions A*, Vol. 35, No. 11, pp. 3595-3603, 2004.

Yaojun Lin, Kevin M. McHugh, Yizhang Zhou and Enrique J. Lavernia, “The Transient to Steady-State Transition during the Spray-Rolling Process”, *Metallurgical and Materials Transactions A*, Vol. 35, No. 11, pp. 3633-3635, 2004.

5.2 Conference Publications and Presentations

S.B. Johnson and J.-P. Delplanque, "Micro-Scale Aspects of Spray Deposition Processing: A Semi-Analytical Model for Droplet Spreading and Solidification at Off-Normal Impact Angles," 2000 ASME IMECE, November 5-10, Orlando, FL, session on Transport Phenomena in Spray and Coating Processes, HTD-Vol. 366-3, Proceedings of the ASME Heat Transfer Division, Vol, 3, pp. 381-388, ASME.

S.B. Johnson, Y. Lin Y. Zhou, J-P Delplanque, and E.J. Lavernia, "Modeling and Simulation of the Spray Rolling Process", *Proceedings of the 2002 International Conference on Process Modeling in Powder Metallurgy & Particulate Materials,* October 28-29 2002, Newport Beach, CA, Alan Lawley, Lyndon Smith and John E. Smugeresky, Editors, pp. 42-50, 2002.

J-P Delplanque, S.B. Johnson, Y. Lin, Y. Zhou, and E.J. Lavernia, "Using CFD Simulation to Improve Spray-Based Materials Processes", *Proceedings of the 2002 International Conference on Process Modeling in Powder Metallurgy & Particulate Materials,* October 28-29 2002, Newport Beach, CA, Alan Lawley, Lyndon Smith and John E. Smugeresky, Editors, pp. 34-41, 2002.

S. B. Johnson and J.-P. Delplanque, "Modeling the Spray-Rolling Process: from droplets to sprays", 39th Annual Technical Meeting of the Society of Engineering Science, Penn State University, PA, October 13-16th, 2002. (Abstract Only).

Sam B. Johnson, Jean-Pierre Delplanque, Enrique J. Lavernia, Yizhang Zhou, Yaojun Lin, Kevin M. McHugh, "Spray Rolling Aluminum Strip: Process Modeling and Parametric Studies", *Proceedings of the TMS 2003, 132 Annual Meeting and Exhibition,* March 2-6-2003, San Diego, CA, pp. 433-441.

Yaojun Lin, Yizhang Zhou, and Enrique J. Lavernia, "*Spray Forming: An Energy Saving and Process Efficient Technique,"* TMS 2003, 132 Annual Meeting and Exhibition, March 2-6-2003, San Diego, CA.

K. M. McHugh, E.J. Lavernia, Y. Zhou, Y. Lin, J.-P. Delplanque, and S.B. Johnson, "Spray Rolling Aluminum Strip--Process Development and Strip Properties," Symposium on Hot Deformation of Aluminum Alloys, 132nd Annual Meeting & Exhibition of TMS, San Diego, California, March 2-6, 2003, pp. 443-452.

J.-P. Delplanque, S.B. Johnson, E.J. Lavernia, Y. Lin, Y. Zhou and K.M. McHugh, "Spray Rolling: A Novel Technique for the Production of Aluminum Strip", *Proceedings of the ILASS Americas, 16th Annual Conference on Liquid Atomization and Spray Systems*, 2003, Monterey, California.

Yaojun Lin, Yizhang Zhou, Sam B. Johnson, Jean-Pierre Delplanque, Kevin M. McHugh, and Enrique J. Lavernia, "On the Selection of Processing Parameters during Spray Rolling Process", *Proceedings of the Second International Conference on Spray Deposition and Melt Atomization (SDMA2003) and the Fifth International Conference on Spray Forming (ICSF V),* June 22-25, 2003, Bremen, Germany, Vol. 2, pp. 7.17-7.30.

Sam B. Johnson, Jean-Pierre Delplanque, Yaojun Lin, Yizhang Zhou, Enrique J. Lavernia, Kevin M. McHugh, "Assisting Spray Rolling Process Development and Scale-up with Modeling and Numerical Simulation", *Proceedings of the Second International Conference on Spray*

Deposition and Melt Atomization (SDMA2003) and the Fifth International Conference on Spray Forming (ICSF V), June 22-25, 2003, Bremen, Germany, Vol. 2, pp. 6.3-6.14.

Kevin M. McHugh, E.J. Lavernia Y. Zhou, Y. Lin J.-P. Delplanque and S.B. Johnson, "Aluminum Strip Processing by Spray Rolling", *Proceedings of the Second International Conference on Spray Deposition and Melt Atomization (SDMA2003) and the Fifth International Conference on Spray Forming (ICSF V),* June 22-25, 2003, Bremen, Germany, Vol. 2, pp. 6.27-6.38.

S.B. Johnson and J.-P. Delplanque, "Simulation Needs in the Modeling of Droplet-Based Processes: The case of spray-rolling", Presented at the Los Alamos National Laboratory Telluride Workshop, Santa Fe, NM, January 21-23, 2003. (Abstract Only)

S. B. Johnson, M. Bussmann, and J.-P. Delplanque, "Modeling and Simulation of Metal Droplet Impact, Spreading, and Solidification on a Solid Substrate", Euromech 450: Studies on Splashes a century after A. M. Worthington, Marseille, France, October 27-29, 2004. (Abstract Only).

Yaojun Lin, Yizhang Zhou and Enrique J. Lavernia, "Mechanisms of Grain size Evolution During Aluminum Spray Forming", *Proceedings of Solidification of Aluminum Alloys,* edited by M.G. Chu, D.A. Granger and Q. Han, March 14-18, 2004, TMS 2004, Charlotte, North Carolina.

S.B. Johnson, J.-P. Delplanque, Y. Lin, Y. Zhou, E.J. Lavernia and K.M. McHugh, "Numerical Simulation and Experimental Characterization of a Binary Aluminum Alloy Spray – Application to the Spray Rolling Process", *Proceedings of the Materials Processing Fundamentals: Solidification & Casting 2005 TMS Annual Meeting*, February 13-17, 2005, San Francisco, CA, pp. 509-517.

Kevin M. McHugh, Y. Lin, Y. Zhou, E.J. Lavernia, J.-P. Delplanque and S.B. Johnson, "Spray Rolling Aluminum Strip for Transportation Applications" *Proceedings of the 6th Global Innovations Symposium: Trends in Materials and Manufacturing Technologies for Transportation Industries: Novel Processes II 2005 TMS Annual Meeting*, February 13-17, 2005, San Francisco, CA.

S. B. Johnson and J.-P. Delplanque, "Resolving Droplet Splashing with Adaptive Mesh Refinement and Accurate Curvature Estimation", 58th Annual Meeting Annual Meeting of the American Physical Society Division of Fluid Dynamics, Chicago, IL, November 20-22, 2005. (Abstract Only)

5.3 Dissertations

S.B. Johnson, *Modeling and Numerical Simulation of Droplet Spreading and Solidification after Impact on a Solid Substrate*, MSc. Thesis, Colorado School of Mines, 2001.

Yaojun Lin, *Reactive Spray and Deposition processes: Fundamental Mechanisms,* PhD Thesis, University of California, Irvine, 2003.

S.B. Johnson, *Droplet Spread, Rebound and Splash*, PhD Thesis, Colorado School of Mines, 2005.

5.4 Technology Transfer

This bench-scale project has demonstrated its potential in commercialization of spray rolling technology. Development of the spray rolling technology through the project was involved by an industrial team and furthermore, has attracted strong interest from potential industrial partners with diversified expertise, including aluminum production, systems engineering in the design and construction of commercial equipment, a world-class manufacturer of twin-roll casting equipment, end-users of aluminum sheet products, and performance evaluation of aluminum sheet products. It is expected that a successful demonstration of process scale-up and steady-state operation, along with verification of anticipated cost and energy savings, will lead to the development of an industry-based pilot-scale facility.

VI. Conclusions and Recommendations

The main objectives of the program were accomplished: (1) Demonstration of process feasibility of a new strip casting method at the bench-scale level; (2) Evaluation of microstructure and material properties of spray-rolled strip; and (3) Scale strip by 2X. The feasibility of the concept of producing aluminum strip by spray rolling was established through the program. In the feasibility study 2124, 3003, 5083, 6111, and 7050 alloys were successfully processed into 100% dense, uniformly flat strip, thereby meeting critical project milestones. For all alloys, a refined microstructure was observed, with a uniform grain structure and uniform distribution of constituent particles. Using temper recipes supplied by industry, analysis of the spray-rolled strip indicated that mechanical properties were at least as good as those of commercial strip, while exhibiting a higher degree of isotropy. Production rates approximately 3X those of commercial twin-roll casters were demonstrated. These important findings demonstrated that spray rolling could eliminate energy-intensive DC casting, hot rolling and homogenization unit operations from commercial ingot-casting practices without sacrificing, and oftentimes improving, material properties due to rapid solidification.

Future technological developments of the spray rolling process can be focused on with the following efforts: (1) to transform spray-rolling technology from current bench-scale to intermediate-scale; (2) to demonstrate steady-state operation of the upgraded spray rolling strip caster; and (3) to reduce energy consumption associated with the manufacture of strip products by eliminating DC casting, homogenization, and hot rolling unit operations in conventional I/M processing.

VII. References

1. Alcoa, *Spray Forming Aluminum: Phase II, Technical Proposal F92-4601-A*. 1992, Alcoa Technical Center.
2. Cochran, C.E. and R.H. McClure, *Automotive Materials Decision: Energy, Economical and Other Issues*, in *SAE Paper No. 820149*.
3. Baker, S. and D. Woodruff, *ALCOA Wants to Take Its Show to the Road*, in *Business Week*. 1994. p. 59.
4. Brown, H.L., B.B. Hamel, and B.A. FHedman, *Energy Analysis of 108 Industrial Processes*. 1996, NJ: Fairmont Press.
5. Bessemer, H. 1865: US 49053.
6. Cole, G.S. and A.M. Sherman, Mat. Charact., 1995. **35**: p. 23.

7. Dieffenback, J.R. and A.E. Mascarin, JOM, 1993(6): p. 16.
8. Li, B.Q., *Producing Thin Strips By Twin-Roll Casting II: Process Modeling and Development.* JOM, 1995(August): p. 13.
9. Lavernia, E.J. and Y. Wu, *Spray Atomization and Deposition*. 1996, Chichester, England: John WIley & Sons.
10. Leatham, A.G., Adv. Mat. Process., 1996(8): p. 31.
11. Leatham, A.G., *Spray forming: alloys, products and markets.* Metal Powder Report, 1999. **54**(5): p. 28-37.
12. Delplanque, J.P., et al. *Using CFD Simulation to Improve Spray-Based Materials Processes*. in *2002 International Conference on Process Modeling in Powder Metallurgy & Particulate Materials*. 2002. Newport Beach, CA.
13. Dai, S.L., J.P. Delplanque, and E.J. Lavernia, *Microstructural characteristics of 5083 Al alloys processed by reactive spray deposition for net-shape manufacturing.* Metall. Mater. Trans. A, 1998. **29A**: p. 2597-2611.
14. McHugh, K.M., et al., *Spray rolling aluminum alloy strip.* Mater. Sci. & Eng. A, 2004. **A383**: p. 96-106.
15. Johnson, S.B., et al. *Numerical Simulation and Experimental Characterization of a Binary Aluminum Alloy Spray - Application to the Spray Rolling Process*. in *Materials Processing Fundamentals: Solidification & Casting 2005 TMS Annual Meeting*. 2005. San Francisco, CA: TMS.
16. Johnson, S.B. and J.-P. Delplanque. *Micro-Scale Aspects of Spray Deposition Processing: A Semi-Analytical Model for Droplet Spreading and Solidification at Off-Normal Impact Angles*. in *2000 ASME IMECE, HTD-Vol. 366-3, Proceedings of the ASME Heat Transfer Division*. 2000: ASME.
17. Johnson, S.B., *Droplet Spread, Rebound and Splash*. 2005, Colorado School of Mines.
18. Johnson, S.B. and J.-P. Delplanque. *Resolving Droplet Splashing with Adaptive Mesh Refinement and Accurate Curvature Estimation*. in *58th Annual Meeting Annual Meeting of the American Physical Society Division of Fluid Dynamics*. 2005. Chicago, IL.
19. Johnson, S.B., et al. *Assisting Spray Rolling Process Development and Scale-up with Modeling and Numerical Simulation*. in *Proceedings of the Second International Conference on Spray Deposition and Melt Atomization (SDMA2003) and the Fifth International Conference on Spray Forming (ICSF V)*. 2004. Bremen, Germany.